SOME

GALVANOMAGNETIC AND THERMOMAGNETIC

EFFECTS ~~PROPERTIES~~ IN N-TYPE

~~OF~~ INDIUM ANTIMONIDE

~~n-TYPE InSb~~

A Thesis submitted for the Degree of M.Phil. in the University of London

by

IMTIAZ AHMAD

ACKNOWLEDGEMENTS

I wish to express my sincere thanks to my supervisor, Dr. R. Mansfield, for the constant guidance and encouragement he has given me during all the problems investigated. I am also grateful to Dr. L. Pincherle for many interesting discussions and suggestions. I would like to thank Professor H.O.W. Richardson, Mr. T.B. Taylor, Dr. N.E. Hill and Dr. J.L. Delany for their kindness and help in connection with the research work.

The co-operation of the technical staff of the Department of Physics at Bedford College is much appreciated. I am particularly grateful to Mr. F.A. Grimes and his colleagues for their valuable help in making the specimen holders.

Finally, I would like to thank Miss A.J. Mills for typing this thesis and making it presentable.

ABSTRACT

D.C. measurements were made of the magnetoresistance and magneto-thermo-electric power to study the Gurevich-Firsov oscillations in n-InSb. The G-F oscillations are quasi-periodic in the reciprocal field. The transverse Nernst-Ettinghausen effect was measured at 91.5°K but the G-F oscillations were obscured by inhomogeneities. The separation of the physical transverse N-E effect from the effect due to inhomogeneities is considered.

Longitudinal and transverse resistivity and Hall coefficient were measured as a function of the electric field at 2.4, 3.1, 3.7, 4.2°K up to 40 KG to study the magnetic freeze out and impact ionisation effects. A comparative study shows that the freeze out effects and the avalanche ionisation are more readily understood from the measurements of longitudinal resistivity rather than from the measurements of transverse resistivity and Hall effect. Assuming that the electrons in the conduction band only contribute to the conductivity the donor ionisation energies as a function of the magnetic field are calculated and compared with the YKA theory. The breakdown field is found to be directly proportional to the calculated donor ionisation energy at 4.2°K.

I N D E X

CHAPTER I

Introduction: Definitions: Experimental Details

1.1 Introduction

In 1961 Gurevich and Firsov [61-G1], [62-F1] predicted that certain transport parameters of semiconductors should vary periodically with the magnetic field due to optical phonon scattering. Their theory was for the non-degenerate case but was later extended to the degenerate case by Efros [62-E1]. The most favourable conditions for the experimental observation of these modulations were discussed by Gurevich, Firsov and Efros [63-G1]. Puri and Geballe [63-P1] were the first to observe Gurevich-Firsov oscillations of magnetoresistance in n-InSb. Their brief report stimulated much interest in the experimental study of Gurevich-Firsov oscillatory effects (G-F effects). There was an avalanche of experimental research papers on this topic. Shalyt, Parfen'ev and Muzhdaba [64-S1], [65-S1] studied G-F oscillations of transverse and longitudinal magnetoresistance in detail. Firsov Gurevich and Parfen'ev [64-F1] reported similar work on magnetoresistance. Muzhdaba, Parfen'ev and Shalyt [65-M1], [66-M1] also reported G-F oscillations of magneto-thermo-EMF in a longitudinal field. Bashirov and Gadzhialiev [67-B1] observed G-F oscillations of transverse Nernst coefficient. Tsidil'kovskii, Aksel and Sokolov [65-T1] studied G-F effects in twenty-five specimens at n-InSb at temperatures from 80°K to 190°K up to 300KG. Their work so much clarified the nature of the oscillations that it reduced interest in further experimental study considerably.

The work for this thesis commenced with the study of G-F oscillations of longitudinal magnetoresistance and longitudinal Nernst-Ettinghausen field. An attempt was also made to observe

G-F oscillations of transverse Nernst-Ettinghausen coefficient but they were obscured by inhomogeneities. Hence the effect of inhomogeneities on transverse Nernst-Ettinghausen effect is considered in detail in Chapter III.

A further development in the study of G-F oscillations arose from the work of Parfen'ev, Farbshtein and Shalyt [68-P1]. They made measurements at 4.2°K in which the electrons were heated by an electric field so that their temperature satisfied the requirements for G-F oscillations. An attempt was therefore made to extend the measurements of Parfen'ev, Fabshtein and Shalyt. The experimental arrangement used to investigate G-F effect was identical to that required for various hot-electron freeze-out effects and the measurements of the freeze-out effects proved so interesting that the original intention of observing G-F oscillations was not pursued.

1.2 Definitions

A current carrying conductor in a magnetic field exhibits certain effects which are known as galvanomagnetic effects. If the primary current is a thermal current instead of an electric current, the transport phenomenon are called thermomagnetic effects

When a magnetic field is parallel to the primary current, the effect is called a longitudinal effect. If the magnetic field is in a transverse direction to that of the primary current, the effect is a transverse effect.

Hall effect, transverse magnetoresistance, longitudinal magnetoresistance, transverse Nernst-Ettinghausen effect and longitudinal Nernst-Ettinghausen effect were measured during the present investigations of n-InSb. Definitions, formulae and units are given in Table 1.1. (Figure 4).

Following the Gerlach [28-G1] convention, the Hall and

TABLE 1.1

Quantity	Symbol	Definition	Laboratory Formula	Units	Remarks
Electrical Resistance	ρ_o	$\left(\frac{E_x}{J_x}\right)_{H=0}$	$\frac{\Delta V_{pp}}{I_x}\ \frac{bt}{l}$	ohm-cm	
Magneto-resistance	ρ	$\frac{\rho(H)-\rho(0)}{\rho(0)}$	$\frac{\rho(H)-\rho(0)}{\rho(0)}$	ohm-cm	
Hall coefficient	R_H	$\frac{E_y}{H_z J_x}$	$\frac{\Delta V_y}{I_x}\ \frac{t}{H_z} \cdot 10^8$	$Coul^{-1} cm^3$	
Transverse Nernst-Ettinghausen coefficient	$Q^{\perp}$	$\frac{E_y}{H_z \frac{dT}{dx}}$	$\frac{\Delta V_y}{\Delta T} \cdot \frac{1}{H_z} \cdot \frac{1}{b} \cdot 10^8$	c.g.s. emu	
Thermoelectric power	$\propto(o)$	$\left(\frac{E_x}{\frac{dT}{dx}}\right)_{H=0}$ or $\frac{1}{e}\frac{E_F}{T}$	$\frac{\Delta V_x}{\Delta T}$	volt $^oK^{-1}$	E_F is electro-chemical potential
Longitudinal Nernst-Ettinghausen Field	E_N^{11}	$[\propto^{11}(H) - \propto(0)]\frac{dT}{dx} = Q^{11}\frac{dT}{dx}$	$\Delta\propto \cdot \frac{\Delta T}{l}$	volt cm^{-1}	
Longitudinal Nernst-Ettinghausen coefficient	Q^{11}	$[\propto^{11}(H) - \propto(0)]_{H=H_x}$	$\frac{\Delta V_x}{\Delta T}(H) - \frac{\Delta V_x}{\Delta T}(0)$	volt $^oK^{-1}$	

Nernst-Ettinghausen effects will be negative if they conform to the polarity shown in Figure 4. Thermo-electric power is positive if the terminal which is connected to the lower temperature region is positive. If the absolute thermo-electric power increases on the application of the magnetic field, the sign of the longitudinal N-E effect will be negative for the electron and positive for the holes.

An effect is an isothermal one if there are no temperature gradients in transverse directions to the direction of primary current, i.e. $\frac{dT}{dy} = \frac{dT}{dz} = 0$.

An effect would be an adiabatic effect if there is no heat flow in the transverse directions to the direction of primary current, i.e. say, $w_y = w_z = o$. Non-dimensional transverse Nernst-Ettinghausen field is defined as

$$E_y = \frac{E_y}{k/e \frac{dT}{dx}}$$

Similarly non-dimensional longitudinal Nernst-Ettinghausen field is defined as

$$E_x = \frac{E_x}{k/e \frac{dT}{dx}}$$

k is Boltzmann constant and e the electronic charge.

1.3 Experimental Details

Superconducting magnet G-452* was used for the G-F oscillations and the transverse N-E effect (Figure 25). The cryomagnetic system had horizontal access to the shields at room temperature, 77°K and 4.2°K, though the shield at 77°K was the only one used during the experiment. Superconducting magnet 1708* was used to

*Oxford Instrument Co., Ltd., Oxford, U.K.

investigate freeze-out effects (Figure 26). This superconducting magnet system had vertical access and could be used only at liquid helium temperatures.

Low temperatures were produced using liquid nitrogen (B.P. 77.3°K) and liquid He^4 (B.P. 4.2°K).

The temperatures below 4.2°K were obtained by lowering the boiling point of liquid helium by reducing the pressure in the liquid helium container. A cartesian automatic pressure controll -er [51-G1] was used to make the temperature constant. At 2.4°K a mercury manometer was used as a vapour pressure thermometer. At 3.1°K and 3.7°K an ordinary barometer tube was used to measure the vapour pressure of the He in the cryostat.

In the temperature range above 77°K T_1-T_2 thermocouples were used. A correction factor for T_1-T_2 thermocouple was worked out from Figure 5. A calibration table for T_1-T_2 thermocouples is prepared (which is given in Appendix II) since no such table is readily available for the research work. A calibration curve for T_1-T_2 is also given in Figure 6 in order to find the temperature difference between two points conveniently and accurately.

It is very difficult to attain isothermal conditions (i.e. $\frac{dT}{dy} = \frac{dT}{dz} = 0$) in the measurements of thermo-magnetic effects since $\frac{dT}{dx} \neq 0$. Pyrophyllite was used in the specimen holder in order to attain the isothermal conditions. Pyrophyllite was machined to form rings of suitable dimensions. The rings were fired at 1100°C for twenty-nine hours which completely drove out the absorbed water and a transformed and harder material was formed. The shrinkage from firing was negligible ($\sim$ 1%). Since a material with iron content gives off gas in a vacuum, the traces of iron in pyrophyllite were investigated by the atomic absorption spectrometer at the Geochemistry Department of the Imperial College

of Science and Technology, London. The maximum iron traces were 0.015% which was considered negligible. Longitudinal Nernst-Ettinghausen effect was studied using this arrangement (Figure 1) and the results were satisfactory.

Single crystals of n-InSb were chosen as specimens for the study of Gurevich-Firsov oscillatory effects and the freeze-out effects for the following reasons:

(i) The crystals cut perpendicular to the crystal growth have a uniform carrier concentration which is of importance in the measurements of transport coefficient.

(ii) n-InSb is a semiconductor with an extraordinarily low effective mass* and a large mobility. The large mobility of carriers increases the amplitude of G-F oscillations and it becomes easier to observe these oscillations.

(iii) G-F oscillations are of weak nature and can be best observed in purer specimens since the purer specimens also result in the large mobility of the carriers. It is noted that n-InSb can be obtained in purer form than other crystals.

(iv) n-InSb is also a suitable specimen for the study of freeze-out effects on account of its purity, low effective mass and a large dielectric constant as described in Chapter IV.

The specimens were supplied by the Ministry of Technology, Electronic Materials Unit, Royal Radar Establishment, Great Malvern, Worcestershire and are listed below:

Specimen	n (cm^{-3}) at $77^{o}K$	$\mu = 0.85R\sigma$ ($cm^{2}V^{-1}sec^{-1}$) at $77^{o}K$
1	4.6×10^{14}	3.7×10^{5}
2	4.9×10^{14}	3.7×10^{5}
3	1.2×10^{14}	4.4×10^{5}

* $m^* = 0.013m_o$

Specimen	n (cm^{-3}) at 77°K	$\mu = 0.85 R_H$ ($cm^2 V^{-1} sec^{-1}$) at 77°K
4	1.4×10^{14}	4.6×10^5
5	4.7×10^{13}	4.6×10^5
6	5.8×10^{13}	5.7×10^5

The specimens were of rectangular shape and the ratio of length to breadth of a specimen was greater than three. The etchant used [64-S1] for ten seconds was

HNO_3	1 part
HF	2 parts
H_2O	3 parts

Freshly cut indium solder with Baker's fluid as flux was used for the soldering of a specimen. The joint was thoroughly rinsed in the distilled water since the Baker's fluid is very corrosive. It was also made sure that the joint formed was not a dry one. The actual procedure adopted to mount the specimens is described below.

(a) Gurevich-Firsov Oscillations

Specimen No. 6 was used to look for G-F oscillations of the longitudinal Nernst-Ettinghausen field and the longitudinal magnetoresistance. The specimen holder used is shown in Figure 1. The dimensions of the specimen were 12.33 x 2.59 x 2.48 mm. The specimen was dipped in methyl alcohol to remove grease from its surface. Etching of the specimen was considered unnecessary as it had naturally good bright surface. The surface was, however, further improved by gently rubbing the specimen on a fine emery paper.

Platinum wire 0.005" diameter (0.127 mm) was used for potential probes. Platinum is generally preferred to Cu as it has a high melting point and does not readily react chemically with other substances. The probes were spot welded [54-M1] using a

40μF capacitor and 14 volts. The final resistance was negligible in each case and the distance between the potential probes was 3.8 mm.

The mean temperature of the specimen was 115°K and the temperature difference between the two ends of the specimen was about 15°K during the measurements of longitudinal N-E effect. In the case of longitudinal magnetoresistance measurements, the temperature difference between the two ends of the specimen was not more than 0.3°K and the mean temperature of the specimen was 102°K.

(b) Transverse Nernst-Ettinghausen Effect

Specimen No. 4 was mounted to look for G-F oscillations of the transverse Nernst-Ettinghausen thermomagnetic effect. The dimensions of the specimen were 11.5 x 3.8 x 3.35 mm. The average distance between electrodes was taken as the length of the specimen for calculations. The specimen was etched after treating with CCl_4. The specimen holder used is shown in Figure 7.

The current to the heater attached to the end of the specimen was switched off when the mean temperature of the specimen was 90.7°K. The temperature of the specimen increased to 92.3°K during the course of observations. The mean temperature of the experiment was 91.5°K. The temperature difference between the two ends of the specimen changed from 21° to 17.13° as the magnetic field was increased from zero to 36kG. The Nernst emf was measured by a Vernier potentiometer (Cambridge Instrument Company No. L-308509) and WPA moving coil galvanometer K-104.

(c) Freeze-out Effects

Specimens 4 and 5 were used to study freeze-out effects. The specimen holder is shown in Figure 9. The specimens were

directly immersed in liquid helium in this case. A valve voltmeter was used to measure the potential difference. The Hall voltage was measured by the usual potentiometer-galvanometer arrangement.

Errors

The estimated errors in the measurements of various quantities are tabulated below in terms of the symbols used in table 2.1.

(a) Measurements at Liquid Nitrogen Temperatures

Quantity	Errors	Total Error
ρ	1% in l; 1% in b; 1% in t; 0.1% in V_{pp}; 0.1% in I_x	1.8%
α	0.3% in V_x; 0.5% in T	0.6%
$Q^{\perp}$	1% in l; 1% in b; 1% in H_z; 0.3% in V_y; 1% in T	2.0%

(b) Measurements at Liquid Helium Temperatures

Quantity	Errors	Total Error
ρ	1% in l; 1% in b; 1% in t; 1% in V_{pp}; 3% in I_x	3.6%
R_H	1% in t; 1% in H; 0.2% in V_{pp}; 3% in I_x	3.3%

CHAPTER II

Gurevich-Firsov Oscillatory Effect

Introduction; Experimental Results; Discussion of Results.

2.1 Introduction

The Gurevich-Firsov oscillatory effect is basically a high magnetic field effect. To observe this effect the magnetic field should be sufficiently strong to satisfy the condition:

$$\omega\tau \gg 1 \qquad \text{(Appendix I)}$$

where ω is the cyclotron angular frequency and τ the electronic relaxation time.

The G-F effect may be understood in terms of the variation of Landau splitting energy with the magnetic field.

When the Landau splitting energy is greater than the energy of the longitudinal optical phonons, coupling between the conduction electrons and the longitudinal optical phonons is weak and the probability of carrier scattering by optical phonons is relatively small. If the magnetic field is gradually decreased, at a certain value of the magnetic field, the Landau splitting energy will become equal to the energy of longitudinal optical phonon and the interaction between the carriers and the optical phonons will be very strong. This will sharply increase the probability of scattering of the conduction electrons by the optical phonon and consequently, for example, transverse magneto conductivity will decrease. On further decreasing the magnetic field the probability of the carrier scattering by the optical phonons will decrease resulting in the increase of transverse magneto conductivity. For a still lower value of magnetic field, the Landau splitting energy will again become equal to the energy of the longitudinal optical phonon which will favour scattering of the electron by the optical phonon and once again will decrease the transverse magneto conductivity.

Hence when the optical modes of the phonon spectrum are sufficiently excited, there will be a large probability of inelastic scattering of the conduction electrons by the phonons for certain resonant values of the magnetic field. The resonance condition is

$$\omega = A\omega_o$$

where ω_o is the angular frequency of the longitudinal optical phonon and A is an integer. The G-F oscillations of the transport coefficients are sometimes called magnetophonon oscillations and the above mentioned resonance as magnetophonon resonance.

Theory predicts that the oscillations are periodic in reciprocal magnetic field with the period

$$\Delta\left(\frac{1}{H}\right) = \frac{e}{m^*\omega_o c}$$

where m^* is the effective mass of electrons and e is the electronic charge.

G-F oscillations can be easily distinguished from Shubnikov-de Haas (S-H) oscillations which are also periodic in reciprocal field with a period given by

$$\Delta\left(\frac{1}{H}\right) = \left(\frac{2e}{\hbar c}\right)\left(3\pi^2 n\right)^{-2/3}$$

where h is Planck's constant and n the carrier concentration. Obviously, the period of S-H oscillations depends on the carrier concentration whereas the period of the G-F oscillations is independent of the carrier concentration.

Puri and Geballe [66-P1] explained the origin of magnetophonon oscillations in a simple manner. The density of states of an electron in a magnetic field is given by

$$N(\epsilon)\,d\epsilon = \left(\frac{1}{2\pi}\right)^2 \left(\frac{k_B^2}{2}\right) \frac{1}{\gamma^{\frac{1}{2}}} \int_{l=0}^{l=l_{max}} \frac{1}{[\epsilon - \hbar(l + \frac{1}{2})\omega_c]^{\frac{1}{2}}}\, d\epsilon$$

where l_{max} is the largest integer for which the condition

$$\epsilon \geqslant (l + \tfrac{1}{2})\,\hbar\omega$$

is satisfied and $k_B^2 = \frac{eH}{\hbar c}$.

Hence when $\epsilon = (l + \frac{1}{2})\hbar\omega$, the density of states, $N(\epsilon)$, is infinite. This infinity in the density of states is the root cause of the G-F oscillations.

In real semiconductors the infinite density of states is limited to a finite density of states and gives rise to extrema on account of the following reasons:

(i) Collision broadening The lifetime of an electron state between two scattering events is finite. This broadens the electron energy levels and the density of states becomes finite. However the condition $\omega\tau \gg 1$ must be satisfied to observe the G-F oscillations.

(ii) Dispersion of phonons The optical phonon of different wavelengths have slightly different energies. This spread in the energy of the phonon limits the amplitude of the oscillations.

The amplitude of oscillations is also determined by the band structure of the semiconductors.

The conduction band of InSb is non-parabolic and consequently the spacing of the Landau levels is not uniform. This reduces the amplitude particularly of higher order oscillations.

Analytical interpretation of the amplitudes of oscillations in terms of collision broadening or phonon dispersion has not been made since it involves too many unknown quantities.

G-F oscillatory effects have been observed experimentally in

non-degenerate materials only, when the Fermi level is below the lowest Landau level. However, theory predicts [62-E1] the occurence of G-F effects in degenerate materials as well. Experimental confirmation is still awaited. The observation of G-F oscillations are expected to be difficult on account of the low mobility of the carriers in a degenerate material. It may be added that Gurevich-Firsov oscillatory effects cannot be observed in certain transport coefficients. For example, Hall effect and the electronic part of the thermo-electric power in a transverse magnetic field do not depend on the scattering of carriers. No G-F oscillatory effects are, therefore, observed in these transport coefficients. Also since the scattering of the carriers by the optical phonons does not contribute to phonon drag, the phonon drag component of magneto-thermo-electric power will not exhibit G-F oscillatory effects.

2.2 Experimental Results

The G-F oscillations of the longitudinal magnetoconductivity and the non-dimensional longitudinal Nernst-Ettinghausen field are shown in Figure 2 and Figure 3 respectively. The resonant oscillations are obtained by finding the difference between an experimental curve and the curve of its monotonic background. The background drawn is the envelope of the maxima or a minima of the experimental curve.

Three minima of the longitudinal magnetoconductivity are reported at H = 32, 17, 11 KG. Comparison of the results with the resonant values of magnetic field obtained by Firsov, Gurevich, Parfen'ev and Shalyt [64-F1] from the measurements of longitudinal magnetoresistance is given in Table 2.1.

Four maxima of non-dimensional longitudinal Nernst-Ettinghausen field are reported at H = 37, 20, 12.7, 8.9 KG. Comparison with the

TABLE 2.1

Resonant Values of the Magnetic Field for the Longitudinal Magnetoresistance $\rho^{//}$, and the Magnetoconductivity, $\sigma^{//}$.

$\rho^{//}$ [64-F1]			$\sigma^{//}$ (Figure 2)		
$H_{(KG)}$	$(\frac{1}{H})$ x 10^{-5} (G^{-1})	$\Delta(\frac{1}{H})$ x 10^{-5} (G^{-1})	$H_{(KG)}$	$(\frac{1}{H})$ x 10^{-5} (G^{-1})	$\Delta(\frac{1}{H})$ x 10^{-5} (G^{-1})
32.5	3.077		32	3.1	
16.5	6.06	3	17	5.9	2.8
11.0	9.09	3	11	9.1	3.2

resonant values of the magnetic field reported by Puri and Geballe [66-P1] is given in Table 2.2.

2.3 Discussion of Results

Figure 2 shows that the measured longitudinal magneto-resistance is positive as the magnetic field is increased from zero to 40.7KG. According to extensive measurements of Tsidil'kovskii, Aksel'rod and Sokolov [65-T1], the longitudinal magnetoresistance of n-InSb is positive up to 4-5KG, then it changes sign and is positive again in fields greater than 100KG in ideal conditions. The absence of negative region in the case of specimen no. 6 may be due to the deviations of the sample from exact parallelism. Since the diameter of the potential probes is 0.127 mm, which is less than the crucial diameter (= 0.3mm) for departure from negative effect, the absence of negative region indicates the presence of inhomogeneities in the specimen.

Periodicity from the first two minima on the strong field side is given by $\Delta(\frac{1}{H}) = 2.8 \times 10^{-5} G^{-1}$. Using $\omega_o = 3.7 \times 10^{13} sec^{-1}$ [62-H1], $m^* = 0.017 m_o$ at 32 KG which is in close agreement with the value of m^* from the cyclotron resonance measurements [61-P1].

From the measurements of longitudinal N-E effect, the periodicity $\Delta(\frac{1}{H}) = 2.3 \times 10^{-5} G^{-1}$ for the first two maxima. Hence the value of $m^* = 0.02 m_o$ at 37 KG which is much higher than given by cyclotron resonance data cited above.

Departure from the exact periodicity is mainly due to the change of effective mass with the magnetic field [61-P1] since the non-parabolic nature of conduction band only limits the amplitude of the extrema.

TABLE 2.2

Resonant values of the magnetic field for longitudinal magneto-thermo emf, $\alpha^{\parallel}$, and non-dimensional longitudinal Nernst-Ettinghausen field, $E^{\parallel}$.

$\alpha^{\parallel}$ [66-P1]			$E^{\parallel}$ (Figure 3)		
H (KG)	$(\frac{1}{H})$ x 10^{-5} G^{-1}	$\Delta(\frac{1}{H})$ x 10^{-5} G^{-1}	H (KG)	$(\frac{1}{H})$ x 10^{-5} G^{-1}	$\Delta(\frac{1}{H})$ x 10^{-5} G^{-1}
42.5	2.35		37.0	2.7	
21.0	4.76	2.41	20.0	5.0	2.3
13.8	7.25	2.49	12.7	7.9	2.9
10	10.0	2.75	8.9	11.3	3.4

CHAPTER III

Transverse Nernst-Ettinghausen Effect

Introduction; Experimental Results and Conclusion.

3.1 Introduction

No single crystal is ideally homogeneous. Inhomogeneities may be in the form of a variation in the impurity concentration. Usually the variation in impurities appears in the form of layers periodically placed in the crystal at the time of its growth. Surface states and the electrical and thermal contacts with a sample may also make a crystal non-homogeneous with respect to its transport properties. Certain transport coefficients are very sensitive to the inhomogeneities [60-H1]. Kudinov and Moizhes [66-K1] studied theoretically the effect of inhomogeneities on the thermomagnetic and galvanomagnetic effects. They found that a large error was introduced in the measurement of the Nernst-Ettinghausen (N-E) coefficient and the transverse magnetoresistance in a strong magnetic field. On the other hand, the Hall constant, the thermal EMF and the longitudinal magnetoresistance are not strongly influenced by inhomogeneities in strong magnetic fields. Drichko and Mochav [66-D1] studied the transverse N-E effect in n-InSb in strong magnetic fields, H, above liquid nitrogen temperatures. They found experimentally that the Nernst-Ettinghausen constant was not inversely proportional to H^2 as predicted by classical theory. It was negative for the high mobility specimens where acoustic scattering predominated. It was positive for low mobility specimens where impurity scattering dominated. The Nernst-Ettinghausen constant in the extreme high fields was positive for nearly all specimens and approached a common limit irrespective of the scattering mechanism. The temperature dependence of the Nernst-Ettinghausen constant also disappeared in fairly strong magnetic fields and it again approached a common value. Since measured

values of the N-E coefficient were larger by several orders of magnitude than the theoretical values, Drichko and Mochav were led to believe that the measured effect in the range of limiting values of the Nernst-Ettinghausen constant is determined by the presence of microinhomogeneities.

Agaev, Mosanov and Ismailov [67-A1] made measurements of the Nernst-Ettinghausen effect in n-type InSb to separate the physical Nernst-Ettinghausen effect from the effect due to inhomogeneities. Their approach is followed in this thesis and is described below.

As the eddy currents due to inhomogeneities interact with the magnetic field, a Hall EMF is superimposed on the measured Nernst-Ettinghausen EMF. If the mean free path of an electron is very much smaller than the mean dimensions of the inhomogeneities, the results obtained do not depend on the relaxation time of the carriers. Hence the true transverse N-E effect and effect due to inhomogeneities are additive and the measured value of N-E coefficient is the sum of the two i.e.

$$Q = Q_p + Q_i \qquad (3.1.1)$$

where Q = measured value of N-E coefficient

Q_i = N-E coefficient due to inhomogeneities

Q_p = physical N-E coefficient

By definition

N-E coefficient due to inhomogeneities $Q_i = \dfrac{E_y'}{H_z \frac{dT}{dx}}$

corresponding Hall constant $R = \dfrac{E_y}{H_z J_x}$

and thermo-electric power $\propto * \dfrac{E_x}{\frac{dT}{dx}}$

the resistivity of homogeneous part of semiconductor $\rho = \frac{E_x}{J_x}$

Therefore $$Q_i = \frac{R \alpha}{\rho} \qquad (3.1.2)$$

This result indicates that Q_i is independent of the field for an impure semiconductor in the weak and strong field limits. In transition regions the dependence of Q_i on magnetic field is governed by dependence of R on H. Ehrenreich [59-E1] and Bate, Willardson and Beer [59-B1] have shown that R depends weakly on H for n-InSb. Q_i, therefore, is nearly independent of H while Q_p decreases in strong field as $\frac{1}{H^2}$. Hence, if Nernst-Ettinghausen effect is measured in n-InSb in weak and strong magnetic fields, the physical effect can be separated from the effect due to inhomogeneities. Physical Nernst-Ettinghausen coefficient, Q_p, is defined by the following equations:

$$Q_p = \pm Q(\text{measured in weak H}) + \mp Q(\text{measured in strong H})$$

and $$Q_p = \pm Q(\text{measured in weak H}) - \pm Q(\text{measured in strong H})$$

The sign of Q_p is positive if measured effect decreases as H is increased and negative if the effect increases when the field is increased.

The sign of Q_i is always negative since it is produced by the Hall effect.

3.2 Experimental Results and Conclusion

The experimental result of the measurements of the transverse Nernst-Ettinghausen thermomagnetic effect is shown in Figure 8. The theory for a homogeneous impure semiconductor demands that the transverse Nernst-Ettinghausen coefficient, Q, should vanish in the strong magnetic fields. Experimentally it is found that Q becomes

negative for strong magnetic fields. This is due to the presence of inhomogeneities in the case of impurity conduction.

The experimental curve shows that

(i) the value of measured Q is positive, and

(ii) the inhomogeneities not only change the magnitude of Q but also its sign.

Figure 8 confirms the experimental results of the measurements of the transverse Nernst-Ettinghausen coefficient by Agaev, Mosanov and Ismailov [67-A1].

CHAPTER IV

Freeze-Out Effects

Introduction: Experimental Results: Discussion of Results

4.1 Introduction

Yafet, Keyes and Adams [56-Y1] (YKA) considered the effect of a strong magnetic field on the impurity states of a solid in terms of a hydrogenic atom model. A parameter, γ, was introduced given by

$$\gamma = \frac{\hbar\omega}{2Ry} \qquad (4.1.1)$$

where ω = the cyclotron frequency of free carriers in a magnetic field

$\frac{1}{2}\hbar\omega$ = zero point energy of the free carriers in a magnetic field

$Ry(=\frac{mZ^2e^4}{2\hbar^2})$ = the energy of the carriers in the lowest state of hydrogen atom with no enternal field.

In a weak magnetic field (i.e. $\gamma < 1$) the magnetic force is small compared with the Coulomb forces. Consequently the magnetic field changes the energy of a state and not the wave function describing the state.

In a strong magnetic field (i.e. $\gamma > 1$), the magnetic forces exceed the Coulomb forces. Since the magnetic forces are centripetal in a plane perpendicular to the magnetic field, the atom contracts in a perpendicular direction to the magnetic field. This increases the magnitude of Coulomb (negative) energy. As a result of this, the ionisation energy of the impurities increases. Hence the charge carriers can be easily trapped in the impurity atoms on account of the increase of the binding energy. For donor impurities, a conduction band may be depopulated by a strong magnetic field and the carriers are said to be frozen out.

For $\gamma = 1$, magnetic field is given by

$$H = 2 \times 10^9 \left(\frac{m^*}{m_o} Z\right)^2 \text{ Oers.} \qquad (4.1.2)$$

where m^* = electron effective mass

m_o = free electron mass

and $Z(= \frac{e}{K})$ = nuclear charge

K being the high frequency dielectric constant of the medium.

Therefore, in order to observe freeze-out effects at low magnetic field, the material should have low effective mass and a large dielectric constant.

$$\text{However, the Bohr radius} = 5.29 \times 10^{-9} \left(\frac{m_o}{m^*}\right) K \text{ cm.} \qquad (4.1.3)$$

Thus a large value of dielectric constant and a low effective mass increases the Bohr radius and the spread of electronic wave functions centred on the impurity atoms increases. Thus freeze-out effects can be best observed in pure materials of low effective mass and a high dielectric constant. Experimental conditions are favourable for the study of such an effect in n-InSb. Keyes and Sladek [56-K1] experimentally confirmed the predicted freeze-out effect in n-InSb.

A quantising magnetic field raises the conduction band by $\frac{1}{2}\hbar\omega$. The strong field also compresses the impurity levels which form a narrow band. This impurity band is not only split off from the conduction band but is also raised by an energy just less than $\frac{1}{2}\hbar\omega$. There is always a finite ionisation energy for the donors of pure n-InSb in a strong field. Sladek [58-S1] made detailed measurements on n-InSb and found that the ionisation energy increased with the magnetic field. The experimentally observed values are less than predicted by YKA theory. This is explained by the finite overlap of electron wave functions even in the most pure specimen. On the hydrogen atom model, the ionisation energy with low magnetic field is given by

$$E = \frac{m^*}{mK^2} \text{ Ry} \qquad (4.1.4)$$

where Ry = 13.6 eV

Therefore, for n-InSb, the ionisation energy of donor = 7×10^{-4} eV. Nasledov [60-N1] and Putley [60-P1] measured the ionisation energy of this order.

Miller [64-M1] thought that the hydrogen atom model was not applicable for n-InSb. He considered the neighbouring impurities in n-InSb in a high magnetic field as hydrogen molecules though they were far apart as compared with lattice spacing. He found a decrease of donor ionisation energy with magnetic field. This could explain the experimental results of Phelan and Love [64-P1] who found that the fraction of electrons ionised at $1^{o}K$ even up to 30 KG might be of the order of 10^{-2}. Beckman, Nanamura and Neuringer [67-B2] found an $H^{1/3}$ magnetic field dependence of binding energy of the magnetically induced bound stated in n-InSb.

Larson [69-L1] repeated calculations of the YKA theory taking into account the non-parabolic nature of conduction band. His results show that the non-parabolic nature of conduction band could not be ignored in calculating the binding energy of the donors. In this way he finds greater ionisation energies of the impurities. For an ultra pure specimen the overlap of impurity sites is shown to be nebligible.

The experimental investigation of freeze-out effects requires a detailed introduction. The freeze-out effects in n-InSb manifest themselves by a rise in the Hall constant as the temperature is reduced indicating a redistribution in the number of free carriers between the conduction band and the impurity band levels. When the temperature is sufficiently low to freeze out carriers and an electric field is applied, it is found that there is a sharp drop in the resistivity at a particular field strength which

is attributed to the avalanche ionisation of the frozen out carriers. The Hall constant also decreases to the value obtained in the exhaustion range. These results have been discussed by Putley [66-P2] using a single band model and an activation energy for the carriers deduced from the Hall effect. A simple two band model has been used by Sladek [58-S1] and also Hanley and Rhoderick [69-H1]. A more sophisticated treatment of the two band model has been given by Miyazawa and Ikoma [67-M1]. They consider two cases corresponding to low and high magnetic fields.

(a) Determination of two-band parameters with a weak magnetic field

Miyazawa and Ikoma assume that the electrons in the conduction band and those in the donor band coexist at liquid helium temperatures even when no magnetic field is applied. They treat conduction in two bands, the conduction band and the impurity band, in terms of relaxation times. The difference between the Hall mobility and the drift mobility is considered negligible. Further, the ratio of the mobilities of the electrons in the two bands is assumed to be constant as the temperature is varied.

The ratio of the carrier concentrations in the two bands depends on the temperature, the electric field and the applied magnetic field. When all the carriers are frozen out, the impurity conduction predominates and the carrier concentration, n_o, is given by

$$R_o = -\frac{1}{n_o e} \qquad (4.1.5a)$$

where R_o is the Hall constant.

When nearly all the electrons are in the conduction band, the carrier concentration, n_o, is again given by

$$R_o = -\frac{1}{n_o e} \qquad (4.1.5b)$$

Between the two extreme cases, the Hall coefficient and the

resistivity, ρ, are given by

$$\frac{R}{R_{exh}} = \frac{(1 + x)(1 + xb^2)}{(1 + xb)^2} \qquad (4.1.6)$$

and $$\frac{\rho}{\rho_c} = \frac{(1 + x)b}{1 + xb} \qquad (4.1.7)$$

where $x = \frac{n_c}{n_i}$, $b = \frac{u_c}{u_i}$, $\rho_c = \frac{1}{n_o e u_c}$, $R_{exh} = -\frac{1}{n_o e}$

$$n_o = n_c + n_i = N_D - N_A,$$

n being the carrier concentration, u, the mobility of carriers and the subscripts c, i, corresponding to the conduction band and the impurity band respectively.

Miyazawa and Ikoma [67-M1] measured the Hall coefficient as a function of electric field in a weak magnetic field. The magnetic field used was sufficiently weak for the resistivity to be practically unchanged. They observed a maximum in the Hall coefficient, R_{max}, which was interpreted as evidence for the two types of carriers participating in the conduction. According to their model the maximum value of the Hall coefficient and resistivity are given by

$$\frac{R_{max}}{R_{exh}} = \frac{1 + b^2}{4b} \qquad (4.1.8)$$

and $$\frac{\rho(E^*)}{\rho_c(E^*)} = \frac{1 + b}{2} \qquad (4.1.9)$$

Where E^* is the electric field at which the R_{max} occurs. They determined the ratio of the mobility of the carriers in the two bands from the equation 4.1.8 or 4.1.9. ρ_c is determined by extrapolating the zero magnetic field resistivity towards the ohmic region as shown in Figure 10. The values of b obtained from equation 4.1.8 and 4.1.9 agreed.

Since at the maximum

$$xb = 1 \qquad (4.1.10)$$

Thus $x = \frac{n_c}{n_i}$ can be found. The results of Miyazawa and Ikoma indicated that the conduction band was relatively empty, even when no magnetic field was applied.

The exact value of n_c in the ohmic region cannot be found since b is not independent of the electric field. However, using the value of R at a particular temperature and the value of b at R_{max}, $\frac{n_c}{n_o}$ and hence n_c can be estimated from the equation 4.1.6.

Since the experimentally determined value of the maximum Hall coefficient as a function of the electric field is the same at various liquid helium temperatures, the value of b will be the same for all such temperatures. Hence $\frac{n_c}{n_o}$ (T) or n_c (T) can be determined. The equation

$$n_c = N_o \, F_{\frac{1}{2}} \left(\frac{\mathcal{E}}{kT}\right) \qquad (4.1.11)$$

gives Fermi energy, $\mathcal{E}$, where $F_{\frac{1}{2}}$ is the Fermi-Dirac integral of the degree $\frac{1}{2}$ and

$$N_o = 4\pi \left(\frac{2m^*k}{h^2}\right)^{3/2} T^{3/2} = 8.08 \times 10^{12} \; T^{3/2} \qquad (4.1.12)$$

is the density of state in the conduction band. The calculated Fermi energy shows that the system can be treated classically. Hence the donor ionisation energy, E_D, and the number of acceptors, N_A, can be calculated from the relation

$$n_c = \frac{n_o}{N_A} \cdot N_c \exp\left(-\frac{E_D}{kT}\right) \qquad (4.1.13)$$

making use of the values of n_c at two different temperatures. Here

$$N_c = \frac{\sqrt{\pi}}{2} N_o$$

and is known as the classical equivalent density of state.

Miyazawa and Ikoma [67-M1] determined the value of E_D which was 60% of the theoretically predicted value as given by Yafet, Keyes and Adams.

(b) Two band parameters with a strong magnetic field

When a strong magnetic field is applied the Hall field increases due to the highly mobile electrons in the conduction band. The Hall coefficient and resistivity are now represented by

$$R_H = \frac{\Sigma\sigma_{12}/H}{(\Sigma\sigma_{11})^2 + (\Sigma\sigma_{12})^2} \qquad (4.1.14)$$

$$\rho_H = \frac{\Sigma\sigma_{11}}{(\Sigma\sigma_{11})^2 + (\Sigma\sigma_{12})^2} \qquad (4.1.15)$$

where $\Sigma\sigma_{nm} = \sigma_{cnm} + \sigma_{inm}$ (4.1.16)

Similarly R_{exh} and ρ_c may be written as

$$R_{exh} = \frac{S_{12}/B}{S_{11}^2 + S_{12}^2} \qquad (4.1.17)$$

$$\rho_c = \frac{S_{11}}{S_{11}^2 + S_{12}^2} \qquad (4.1.18)$$

where S_{nm} may be connected with σ_{cnm} by

$$\sigma_{cnm} = \left(\frac{n_c}{n_o}\right) S_{nm} = \frac{x}{1+x} S_{nm} \qquad (4.1.19)$$

There is, in fact, no difference between σ_{cnm} and S_{nm} except for the carrier numbers.

Hence equations 4.1.6 and 4.1.7 are replaced by

$$\frac{R}{R_{exh}} = \frac{\rho^2 + (RH)^2}{\rho_c^2 + (R_{exh}H)^2} X + \frac{\rho^2 + (RH)^2}{\rho_c^2} \frac{1 - X}{b^2} \qquad (4.1.20)$$

and $$\frac{\rho}{\rho_c} = \frac{\rho^2 + (RH)^2}{\rho_c^2 + (R_{exh}H)^2} X + \frac{\rho^2 + (RH)^2}{\rho_c^2} \left(\frac{1 - X}{b}\right) \qquad (4.1.21)$$

Here $X = \frac{x}{1 + x} = \frac{n_c}{n_o}$.

X (or $\frac{n_c}{n_o}$) and b are determined by simultaneously solving equations 4.1.20 and 4.1.21 at a particular magnetic field. Miyazawa and Ikoma plotted $\frac{n_c}{n_o}$ as a function of magnetic field which showed that n_c increases to a maximum value before an appreciable freeze-out takes place as predicted in the original YKA theory.

On lowering the temperature below 4.2°K, it is found that

(a) $\rho_c \left(= \frac{1}{n_o e u_c}\right)$ remains practically constant,

(b) b may slightly increase, and

(c) u_i shows a logrithmic decrease.

Since u_i becomes very small in very strong magnetic fields, it indicates that donor band is very narrow and E_D can be calculated more accurately than the low magnetic field observations. The Fermi energy, ζ, can now be calculated from the relation:

$$n_c = N_B F_{-\frac{1}{2}} \left(\frac{\zeta}{kT}\right) = \frac{N_D}{1 + \exp\left(E_D + \zeta\right)/kT} - N_A \qquad (4.1.22)$$

where $N_B = (2\pi m^* kT)^{\frac{1}{2}} \frac{eH}{h^2 c} = 3.67 \times 10^{10} HT^{\frac{1}{2}}$ (4.1.23)

in Gaussian units.

If classical statistics apply, then equation 4.1.22 can be replaced by

$$n_c = \frac{n_o \sqrt{\pi}}{N_A} \exp\left(- \frac{E_D(B)}{kT} \right) \qquad (4.1.24)$$

and E_D and N_A are determined from this equation. The values of E_D so obtained are compared with theoretically predicted values. Since $N_D - N_A$ is known, N_D can be determined.

However $$N_D = \frac{4\pi}{3} r^3$$

Hence one-half the mean donor distance, r, can be worked out. r can also be determined by plotting the donor band mobility against the square of the reciprocal of the reduced radius of a donor wave function in a direction perpendicular to the magnetic field. This curve approaches to an exponential line at the lower liquid helium temperatures and the donor band mobility tends to be proportional to exp $(- \frac{\text{constant}}{a_1^2})$. This constant is taken equal to $\frac{1}{2r^2}$ in accordance with the treatment of Sladek [58-S1]. Hence the slope of the exponential line gives another value of r. The agreement between the values of r obtained in the two different ways mentioned above supports the approach of this analysis.

Miyazawa and Ikoma also investigated the non-linear quantum limit effects in n-InSb. A minima in the resistivity is observed as predicted by Kazarinov and Skobov [62-K1] at electric fields of the order of 30 volt/cm. In this, the electrons are heated by the large electric field until their temperature, T_e, destroys the quantum limit and

$$kT_e > \hbar\omega$$

Below the field resistivity decreases as impurity scattering is predominant (τ = const. $E^{3/2}$). Above the field the electrons would be scattered by phonons (τ = constant $E^{-\frac{1}{2}}$) and resistivity increases.

The result of this analysis is represented in the following typical figure.

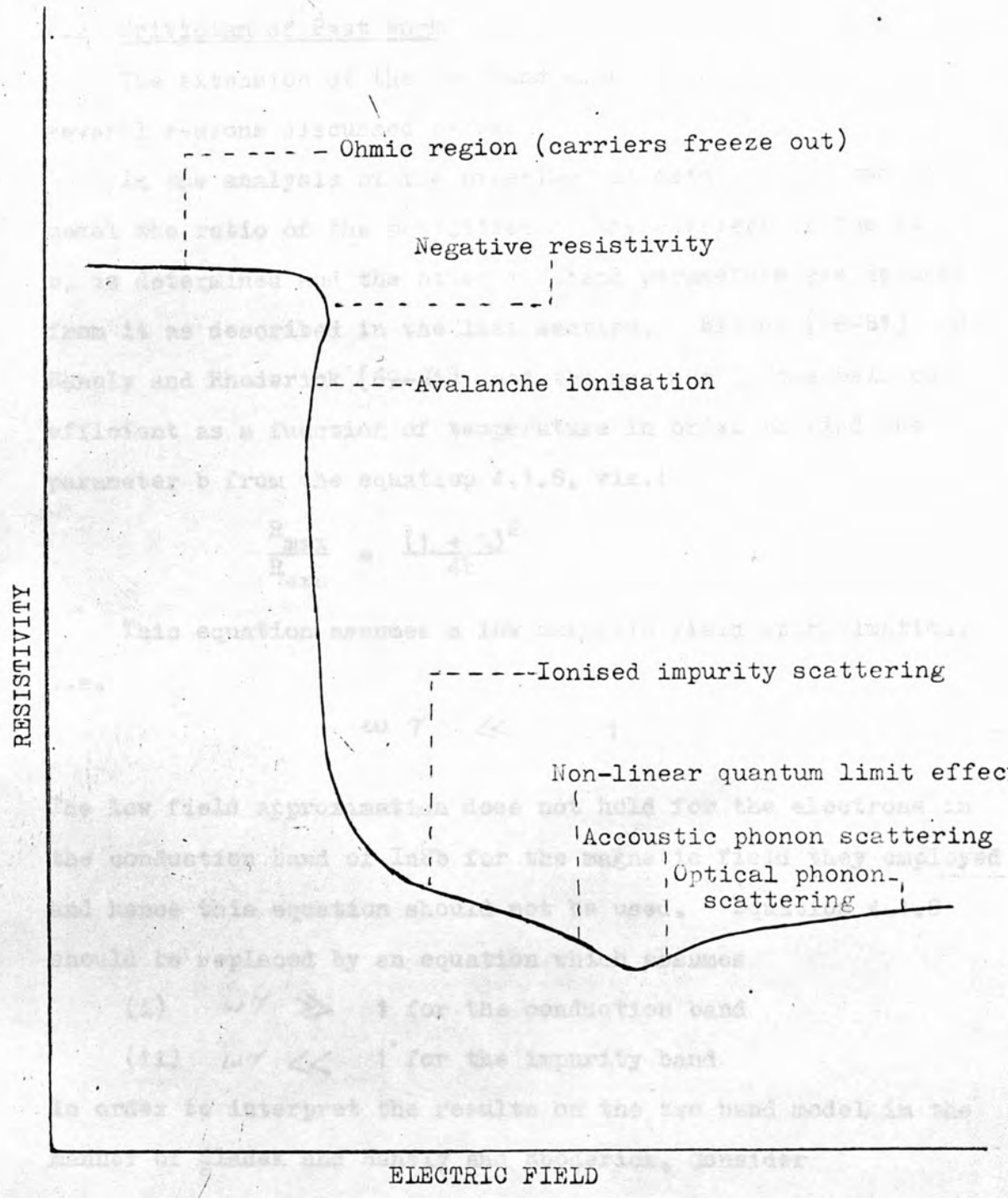

Figure VARIATION OF RESISTIVITY WITH ELECTRIC FIELD AT LIQUID HELIUM TEMPERATURES IN n-InSb

4.2 Criticism of Past Work

The extension of the two band model to InSb is dubious for several reasons discussed below.

In the analysis of the experimental data using a two band model the ratio of the mobilities of the carriers in the two bands, b, is determined and the other two-band parameters are deduced from it as described in the last section. Sladek [58-S1] and Hanely and Rhoderick [69-H1] used the maximum in the Hall coefficient as a function of temperature in order to find the parameter b from the equation 4.1.8, viz.:

$$\frac{R_{max}}{R_{exh}} = \frac{(1 + b)^2}{4b}$$

This equation assumes a low magnetic field approximation, i.e.

$$\omega \tau \ll 1$$

The low field approximation does not hold for the electrons in the conduction band of InSb for the magnetic field they employed and hence this equation should not be used. Equation 4.1.8 should be replaced by an equation which assumes

(i) $\omega\tau \gg 1$ for the conduction band

(ii) $\omega\tau \ll 1$ for the impurity band

in order to interpret the results on the two band model in the manner of Sladek and Hanely and Rhoderick. Consider

$$E_y = - \frac{D_c + D_i}{(A_c + A_i)^2 + (D_c + D_i)^2} J_x$$

where $D = \frac{ne^2\tau}{m^*} \frac{\omega\tau}{1 + (\omega\tau)^2}$

and $A = \frac{1}{\omega\tau} D$

Now for the conduction band

$$D_c = \frac{n_c e^2}{m^* \omega_c} = \frac{n_c ec}{H}$$

and $A_c \ll D_c$

For the impurity band,

$$D_i \ll A_i$$

and $$A_i = \frac{ne^2\tau}{m^*} = \bar{n}_i u_i e$$

$$E_y = - \frac{\frac{n_c eC}{H} + \frac{n_i u_i eH}{c}}{(\bar{n}_i u_i e)^2 + (\frac{n_c eC}{H})^2} \cdot J_x$$

where A_c is neglected compared to A_i

Therefore $$R = - \frac{n_c eC + n_i \frac{u_i^2 eH^2}{C}}{(\bar{n}_i u_i eH)^2 + (n_c eC)^2}$$

Limit $n_i \longrightarrow 0$

$$R = - \frac{1}{n_c ec}$$

Limit $\bar{n}_c \longrightarrow 0$

$$R = - \frac{1}{n_i ec}$$

General Case

$$R = - \frac{1}{ec} \frac{n_c + n_i \omega^2 \tau^2}{n_c^2 \omega^2 \tau^2 + n_c^2}$$

Let $\omega^2 \tau^2 = a$

$$-R = \frac{1}{ec} \frac{n_c \pm (n_o - n_c)a}{(n_o - n_c)^2 + n_c^2}$$

The condition for a maxima for the Hall coefficient is given by

$$n_c^2 (a - 1) - \bar{n}_c 2n_o a + n_o^2 a = 0$$

$$\frac{n_c}{n_o} = \frac{a \pm \sqrt{a}}{a - 1} = \frac{\omega\tau (1 \pm \omega\tau)}{(\omega\tau)^2 - 1}$$

$$= \frac{\omega\tau}{\omega\tau - 1} \quad \text{or} \quad \frac{\omega\tau}{\omega\tau + 1}$$

The second alternative gives a positive n_c.

Substituting in the original expression for R and assuming that $n_c = n_o \frac{\omega\tau}{\omega\tau + 1}$

and $n_i = n_o - n_c = n_o \frac{1}{\omega\tau + 1}$

$$R_{max} = \frac{1}{n_o e c} \frac{\frac{\omega\tau}{\omega\tau + 1} + \frac{\omega^2\tau^2}{\omega\tau + 1}}{\frac{\omega^2\tau^2}{(\omega\tau + 1)^2} + \frac{\omega^2\tau^2}{(\omega\tau + 1)^2}}$$

$$R_{max} = \frac{(\omega\tau + 1)^2}{n_o e C} \quad \frac{1}{2\omega\tau}$$

$$\frac{R_{max}}{R_{exh}} = \frac{(\omega\tau + 1)^2}{2\omega\tau} \qquad (4.2.1)$$

Expression (4.2.1) gives $u_i = 7$ cm^2/volt-sec for $\omega\tau \ll 1$ at H = 43KG using Hanely and Rhoderick's results. On the other hand when H = 43KG assuming $u_c = 10^5$cm^2/volt-sec, and using expression (4.1.8), u_i will be equal to 160 cm^2/volt-sec for the same data. u_i would in fact be much less than this value.

In the two band model it is assumed that the impurity levels merge into a band in a strong magnetic field. The conduction in the impurity band is then described as in the conduction band in terms of a relaxation time and an electronic effective mass. However, for the situations in which the model has been applied the concentration of donors and acceptors are of the order $10^{14}cm^{-3}$, corresponding to an average impurity separation of $10^{-5}cm$. Treating such a widely spaced lattice of impurities as giving rise to a band with normal scattering of carriers seems very doubtful. The work on germanium although more extensive and detailed was not pursued using the two band model to the same extent. Thus Hung [50-H1] originally deduced a mobility of between 10^{-4} and $100cm^2$/volt sec but in the much more detailed work of Fritzsche [55-F1] with far more results than those obtained by InSb, the analysis was not carried out to the same extent. In fact more recent work has concentrated on analysing the conduction by impurities as a hopping process. It has been observed that a transition from an impurity band type process to a hopping process occurs for a certain range of concentrations of impurities in germanium and silicon. For silicon this transition region is 10^{18} - $10^{19}cm^{-3}$ and for germanium 10^{16} - $16^{17}cm^{-3}$. A maximum is observed in the Hall coefficient when the temperature is decreased, both above and below these concentrations. Hence the maximum in the Hall coefficient is not evidence for impurity band conduction. The transition region for InSb will occur at a lower concentration as the Bohr orbits are much larger than for germanium or silicon. The orbits, however, contract considerably in a strong magnetic field and the conduction due to the frozen out electrons is more likely to be by hopping.

The kinetic approach breaks down when

$$\tau < \frac{\hbar}{kT}$$

$$\text{or} \quad \tau < 10^{-11} \text{ sec.}$$

But at $4.2^{\circ}K$ $\tau > 2 \times 10^{-12}$ sec, as given by $u = 7 cm^2/volt\ sec$.

The mean free path of the carriers becomes short for low mobilities and may be comparable with interatomic spacing.

The suggestion in the work of Miyazawa and Ikoma [67-M1] and other similar works, that the field accelerating the electron is the sum of the Hall and applied field is also doubtful. It would suggest that in the longitudinal configuration, the field required to produce impact ionisation should be much greater. The present work was carried out to test this.

It was, therefore, necessary, to measure the longitudinal mangetoresistance, when no Hall field is present, to look for the behaviour of the frozen out electrons. It was also necessary to measure the transverse magnetoresistance and the Hall coefficient to compare the results with other authors.

4.3 Experimental Results

The variation of longitudinal resistivity with the electric field is shown in Figures 10 and 11 for specimen 5 and in Figures 14 and 15 for specimen 4. The variation of the Hall coefficient with the electric field is represented by Figures 21 and 22 and the simultaneously measured transverse resistivity by Figures 12, 13, 16 and 17. The variation of longitudinal and transverse resistivity with the magnetic field is shown in Figures 18 and 19.

4.4 Discussion of Results

Figures 10 - 17 show the variation of resistivity with the electric field of specimens 4 and 5 with and without a magnetic field. It is noted that:

1. The variation of resistivity at a particular magnetic field practically obeys Ohm's law for low values of electric field. The resistance is, however, very much increased by the application of a magnetic field or by lowering the temperature of the specimen. It is due to the freeze-out of carriers on account of the increase of their ionisation energy as predicted by YKA theory.

2. For a strong enough electric field, the frozen-out electrons are excited back into the conduction band by the avalanche impact ionisation. As a result of this, the resistance drops by several orders of magnitudes. This sudden drop of resistance is accompanied by negative resistance at high magnetic fields. The purer the specimen the lower the magnetic field required to observe such a negative resistance.

3. The breakdown field to cause avalanche ionisation increases with the magnetic field. Comparison of Figures 10 - 11 with Figures 12 - 13 for specimen 5 shows that for a particular magnetic field the breakdown field is lower for the longitudinal configuration than the transverse one both at 4.2°K and 2.4°K. Comparison

of Figures 14 - 15 with Figures 16 - 17 shows that the same is true for specimen 4. This result differs from the suggestion in the work of Miyazawa and Ikoma [67-M1] that the field accelerating the electron is the sum of the Hall field and the applied field resulting in a greater breakdown field in the longitudinal case than in the transverse one.

4. There is some freeze-out of the carriers even in the absence of the magnetic field as observed by Miyazawa and Ikoma. Zero field freeze-out is enhanced with the decrease of temperature or impurity concentration like magnetic freeze out. The zero field resistivity in the absence of freeze out is obtained by extrapolating resistivity vs. electric field curve from the avalanche ionisation towards the lowest value of the electric field and ignoring the sudden drop of resistance. This value is 0.26 and 1.4 ohm-cm for specimens 4 and 5 respectively.

5. Figures 10 and 11 show that the longitudinal resistivities at different magnetic fields approach a common curve at high electric fields when $\angle N_D - N_A$ electrons of specimen 5 are $\angle$ in the conduction band; where N_D is the number of donors and N_A is the number of acceptors. Figures 14 and 15 show that specimen 4 also behaves in exactly a similar manner. This suggests that, when no Hall field is present, the mobility of carriers in the conduction band is independent of the magnetic field which agrees with the predictions of Adams and Holstein [59-A1] and Kubo et al. [65-K1]. Hence the changes of resistivity on the application of the magnetic field is due to the changes of carrier concentration in the conduction band.

6. Zero field resistivity vs. electric field curves for a particular specimen at 4.2°K and 2.4°K (Figures 10 and 11) further suggest that the mobility of the carriers in the conduction band is also nearly independent of the temperature. The field-independent

and temperature-independent mobility of the carriers in the conduction band estimated from the extrapolated zero field resistivity is 1.718×10^5 and 0.95×10^5 $cm^2/volt^{-1}sec^{-1}$ for specimens 4 and 5 respectively.

7. Figures 12, 13, 16 and 17 show that transverse resistivity curves do not converge after impact ionisation to zero field curve, thus indicating a magnetic field dependence of this mobility. Though the transverse resistivity is always greater than the longitudinal resistivity, it closely follows the variation of longitudinal resistivity. The difference between the two becomes very small at the highest magnetic fields and the lowest temperatures employed as shown in Figure 20. This would be predicted in the elementary theory for conduction in a single band in the high field limit as shown in Appendix III. It is obvious that the experimental data of longitudinal resistivity can be more readily analysed than the data of transverse resistivity to interpret the freeze-out effects and the breakdown field.

Now consider the variation of resistivity with magnetic field. Figure 18 shows that the variation of longitudinal resistivity with the magnetic field for both the specimens is the same except for a numerical constant. Figure 19 shows that it is also true for the transverse resistivity of the two specimens. It appears that the numerical constant is equal to the square of the ratio of total number of carriers i.e.

$$\sigma = \left[\frac{(n_o)_4}{(n_o)_5}\right]^2 f(H)$$

where $n_o = N_D - N_A$ and f (H) is a rapidly varying function of the magnetic field but is the same for different concentrations and temperatures. This does not seem to be consistant with a two band model. In the two band model the electrons are distributed between the two bands (conduction band and donor band) according

to the temperature and magnetic field, and the conductivity is equal to the sum of the contributions from the two bands. The contribution to conductivity from each band depends upon the number of carriers and their mobility in that band. But the identical variation of longitudinal as well as transverse resistivities of the two specimens strongly suggests that the resistivities are determined by one common factor rather than the contributions from two bands depending upon the relative carrier concentration between them and the relevant mobilities in the two bands. Hence the two band model is not suitable to interpret the freeze-out effects in n-InSb.

The following is a description of how N_D and N_A are determined. In order to check the degeneracy of the specimen, the reduced Fermi energy was calculated from the relation [59-P1]

$$n = \frac{4\pi(2m^*kT)^{3/2}}{h^3} F_{\frac{1}{2}}(\eta^*)$$

$$= 5.45 \times 10^{15} (m^*/m)^{3/2} T^{3/2} F_{\frac{1}{2}}(\eta^*)$$

The specimens are partially degenerate at higher temperatures but are degenerate at lower temperatures. R. Mansfield [56-M1] has developed the theory of impurity scattering in semiconductors for the general case of arbitrary degeneracy. The equation for the conductivity due to impurity scattering is given as

$$\sigma_I = \frac{32 K^2 m^* (kT)^3 f_2(\eta^*)}{N_D e^2 h^3 f(x)}$$

where $$f(x) = \ln(1 + x) - \frac{x}{1 + x}$$

$$x = \frac{\bar{\eta}(kT)^{\frac{1}{2}} K h}{e^2 (2m^*)^{\frac{1}{2}} f_{\frac{1}{2}}(\eta^*)}$$

The value of $\bar{\eta}$ can be conveniently obtained from the graph

shown in Figure 27. The extrapolated value of was used in this calculation.

Since all the quantities are known, N_D can be calculated.

Since $N_D - N_A$ is obtained from the measurements of the Hall coefficient at 77^oK, N_A is easily found and is given in Table 4.1.

TABLE 4.1

Specimen	$N_D - N_A$ x 10^{14} (cm^{-3})	N_D x 10^{14} (cm^{-3})	N_A x 10^{14} (cm^{-3})
4	1.4	3.7	2.3
5	0.47	3.9	3.43

In the light of the above conclusions and calculations, the model considered for the evaluation of donor ionisation energy is:

(i) The experimental data of the longitudinal conductivity, with no Hall field is preferred to the experimental data of transverse conductivity for the calculation of donor ionisation energy.

(ii) Only the electrons in the conduction band contribute to conductivity.

(iii) Mobility of carriers in the conduction band is independent of magnetic field.

(iv) Mobility of carriers in the conduction band is also nearly independent of temperature.

(v) Impurity scattering is the dominant scattering mechanism even in the event of freeze out.

Longitudinal conductivity, $\sigma^{\parallel}$, is given by

$$\sigma^{\parallel} = n e u = \frac{n_o N_c}{N_A} \exp\left(-\frac{E_D}{kT}\right) e u$$

Where n = density of electrons in the conduction band

u = mobility of electron in the conduction band

$$N_c = (2\pi m^* kT)^{\frac{1}{2}} \frac{eH}{h^2 c} \quad \text{in Gaussian units}$$

$$= 3.67 \times 10^{10} HT^{\frac{1}{2}}$$

It is assumed that $n \ll n_o$ and $n \ll N_A$.

Table 4.2 gives the values of E_D determined in this way.

Values of E_D at a fixed magnetic field are remarkably consistent for the two specimens at different temperatures. The mean values of E_D (with the exception of 2.4^oK) are shown in Figure 23 along with the theoretical values of YKA and Putley's experimental results. Theoretical values are larger than the experimental values obtained here since the YKA theory is for an isolated hydrogen atom and the donors of the specimens used are not isolated. Fenton and Haering [67-F1] and Durkan et al. [68-D1] have shown that the ionisation energy may be considerably less than that predicted by YKA theory. It should, however, be noted that the activation energy calculated here would be larger if impurities also contribute to the conduction.

On the simple picture considered here, the Hall coefficient should increase at the same rate as the longitudinal magnetoresistance increases with the magnetic field. Figure 19 shows that it is not the case. The Hall effect results are, therefore, inconsistant with the model described. If

$$u = 10^5 \text{ cm}^2/\text{volt sec}$$

$$H = 40 \text{ KG}$$

The Hall angle $\frac{RB}{\rho_\perp} = \omega\tau$, on the single model, would be as large as 40. The value of the Hall angle, for example, for

TABLE 4.2

Ionisation energy E_D and Breakdown field E_c

B kG	Specimen 4 E_D meV 4.2°K	3.7°K	3.1°K	2.4°K	$cm^{-1}coul^{-1}$ E_c/E_D 4.2°K	Specimen 5 E_D meV 4.2°K	3.7°K	3.1°K	2.4°K	$cm^{-1}coul^{-1}$ E_c/E_D 4.2°K
40	3.0	3.0	2.8	2.4	197	3.1	3.2	3.0	2.7	297
30	2.6	2.6	2.5	2.2	196	2.7	2.8	2.6	2.4	287
20	2.1	2.1	2.1	1.8	186	2.3	2.3	2.1	2.1	289
10	1.4	1.4	1.4	1.2	180	1.6	1.6	1.5	1.4	280
5	0.85	0.84	0.80	0.64		1.	1.0	0.93	0.86	

specimen 5 was 0.52 at 40KG. The theoretical and experimental values of the Hall angle do not agree.

Note that a Hall angle of the order of 40 would be difficult to measure experimentally as it would distort the equipotential lines considerably. The large Hall angle may also lead to the non-ohmic behaviour of the Hall coefficient on account of the high local electric field. It is not clear whether the inconsistency of the results of the Hall coefficient is due to the experimental technique or whether the theory for the Hall effect in the extreme quantum limit needs revision.

The values of the Hall angle experimentally obtained were, however, remarkably independent of the magnetic field at a particular temperature with the exception of 2.4^{o}K as shown in Table 4.3.

TABLE 4.3

Experimental Values of Hall angle

SPECIMEN 4

H (KG)	$\frac{RH}{\rho_\perp}$			
	4.2°K	3.7°K	3.1°K	2.4°K
10.1	1.21	0.88	0.76	0.51
20.1	1.18	0.87	0.66	0.46
30.2	1.17	0.85	0.59	0.27
40.3	1.08	0.71	0.47	0.17

SPECIMEN 5

H (KG)	$\frac{RH}{\rho_\perp}$			
	4.2°K	3.7°K	3.1°K	2.4°K
5.0	--	0.43	--	0.194
10.1	0.546	0.44	0.358	0.22
20.1	0.556	0.47	0.366	0.22
30.2	0.55	0.44	0.34	0.14
40.3	0.52	0.43	0.285	0.1

CONCLUSIONS

The Gurevich-Firsov oscillations of longitudinal magneto-conductivity and longitudinal N-E field in n-InSb are not exactly periodic in reciprocal field on account of the variation of the effective mass with the magnetic field.

The transverse N-E effect is completely determined by inhomogeneities in a strong magnetic field and the G-F oscillations can be easily obscured by the inhomogeneities. The physical trans-verse N-E effect can be separated from the effect due to inhomogeneities using the experimental observations.

The study of freeze-out effects in InSb shows that there is some freeze out of carriers even in the absence of magnetic field. The magnetic freeze-out and breakdown field which causes impact ionisation can be interpreted more readily with a longitudinal configuration than the transverse one. It is found that the frozen out electrons do not contribute to the conductivity. The mobility of carriers in the conduction band is independent of magnetic field and temperature. The calculated donor ionisation energy compares favourably with the YKA theory. The breakdown field is found to be proportional to the calculated donor ionisation energy at $4.2^{o}K$. The Hall effect results cannot be satisfactorily explained on this model and it is not clear whether the discrepancy is due to the measurement technique or theory.

APPENDIX I

Criterion for weak and strong magnetic field [62-T1]

The effect of magnetic field on charge carriers does not only depend upon the intensity of magnetic field, H, but also on the carrier mobility, u. Further, the transport coefficients depend more on magnetic field in a weak field as compared with a strong field.

Consider the motion of an electron at right angles to a constant magnetic field H_z :

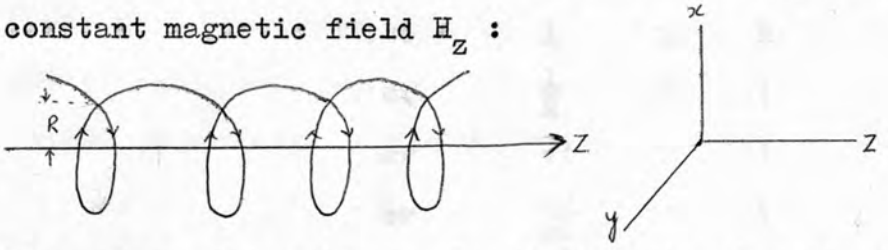

The radius of curvature, R, of the helical path of the electron is

$$R = \frac{cm^*v}{eH}$$

$$= \frac{v}{w}$$

where $w = \frac{eH}{m^*c}$ called cyclotron frequency. It is the angular frequency of revolution of electron in the xy plane.

v = projection of electron velocity on xy plane

e = absolute value of the charge of electron

m^* = effective mass of electron

Let l = mean free path of electron

and t = mean free time or mean time between two collisions

Consider two cases:

(a) Where $l \ll R$

or $t \ll \frac{1}{w}$

At the end of time, t, the direction of motion of the electron will make an angle with the initial direction of motion. This angle, θ , between the initial and final directions of motion before and after the collision is given by

$$\theta = \frac{l}{R} = wt$$

Now weak fields are those fields for which this angle is small. They produce only a small change in the direction of motion of carrier at the end of time interval t .

(b) Strong fields bring about large changes in θ.

i.e. $l \gg R$

or $\frac{l}{R} \gg 1$

or $wt \gg 1$

or $\frac{eH}{m^*c}t \gg 1$

but $\frac{et}{m^*} = u$, the mobility of carriers. Hence the condition for a strong magnetic field is

$$\frac{uH}{c} \gg 1$$

It is obvious that not only the intensity of the magnetic field, but also the mobility of the carriers, must be taken into account to name a field weak or strong. A strong field for electron-current is not a strong field for hole-current of the same material on account of the different effective masses of an electron and a hole.

Usually, the criterion for strong magnetic field is taken as

$$(\frac{uH}{c})^2 \gg 1 \qquad (1)$$

since this inequality is satisfied at lower values of H than $\frac{uH}{c} \gg 1$.

Similarly, for weak magnetic fields the criterion would be

$$(\frac{uH}{c})^2 \ll 1 \qquad (2)$$

Conditions (1) and (2) would hold good for quadratic isotropic law (i.e. $\epsilon = \frac{p^2}{2m^*}$) as well as for quadratic

anisotropic dispersion law [e.g. $\epsilon = \frac{1}{2}(\frac{p_1^2}{m_1^*} + \frac{p_2^2}{m_2^*} + \frac{p_3^2}{m_3^*})$].
For other dispersion laws the two criteria would be more true in the following simpler form:

$$\frac{uH}{c} \gg 1 \quad \text{for strong magnetic fields}$$

$$\frac{uH}{c} \ll 1 \quad \text{for weak magnetic fields}$$

Relations (1) and (2) can be further improved if we write mobility in the form

$$u = \frac{e\tau}{m^*}$$

Where τ is mean free time required to cover mean free path obtained by averaging statistically through the statistical weight of carrier energy, ϵ, for each particle, i.e.

$$\tau = \frac{\langle \epsilon t \rangle}{\langle \epsilon \rangle}$$

Here brackets indicate an average over the Maxwell Boltzmann distribution:

$$\langle x \rangle = \frac{\int_0^\infty x \epsilon^{\frac{1}{2}} e^{-\frac{\epsilon}{kT}} d\epsilon}{\int_0^\infty \epsilon^{\frac{1}{2}} e^{-\frac{\epsilon}{kT}} d\epsilon}$$

As u depends on τ while τ depends on ϵ, the carrier energy. Thus the importance of various scattering mechanisms will depend upon the carrier energy. Suppose there are two scattering mechanisms present simultaneously. If mean free time (m.f.t.) for principal scattering mechanism is τ and m.f.t. for additional scattering mechanism is τ_1, then the effective m.f.t., τ^*, for total probability of scattering is given by:

$$\frac{1}{\tau^*} = \frac{1}{\tau_1} + \frac{1}{\tau}$$

If $\tau_1 > \tau(kT)$, i.e. the value of τ when $\epsilon = kT$, then additional scattering mechanism will be only important in weak field. It should be ignored in the strong field.

If the value of the carrier energy, say, $\epsilon' < kT$

then $\tau_1(\epsilon') \doteq \tau(\epsilon')$

and $\tau^*(\epsilon') \gg \tau(kT)$ i.e. the value of τ when $\epsilon = kT$.

though $\tau^*(\epsilon') = \tau(\epsilon')$

therefore $\tau(\epsilon') \gg \tau(kT)$ (3)

Therefore the criterion of strong magnetic field should be

$$\left(\frac{\tau(\epsilon')}{\tau(kT)}\frac{uH}{c}\right)^2 \gg 1 \quad (4)$$

or $$\left(\frac{u'}{c}H\right)^2 \gg 1 \quad (5)$$

where $u' = \frac{e\tau(\epsilon')}{m^*}$ called effective mobility.

u' is supervised by m.f.t. $\tau(\epsilon')$.

Similarly criterion for weak magnetic field is:

$$\left(\frac{\tau(\epsilon')}{\tau(kT)}\frac{uH}{c}\right)^2 \ll 1 \quad (6)$$

or $$\left(\frac{u'}{c}H\right)^2 \ll 1 \quad (7)$$

Relations (3) and (6) show that more dependence of transport coefficients upon the intensity of magnetic field should appear in weak magnetic field than that given by $\left(\frac{uH}{c}\right)^2 \ll 1$, the ordinary inequality.

To sum up, when $\left(\frac{u'}{c}H\right)^2 \gg 1$, the principal scattering mechanism is dominant. When $\left(\frac{u'}{c}H\right)^2 \lesssim 1$, the principal as well as the subsidiary mechanisms are present and both cannot be ignored. In this case the dependence of relaxation time on the carrier energy cannot be given by usual power function of carrier energy, i.e.

$$\tau = \tau_0(T)\left(\frac{\epsilon}{kT}\right)^{r-\frac{1}{2}}$$

where $\tau(T)$ and r have different values for different scattering mechanisms.

APPENDIX II

Calibration Table for the British Chromel Alumel (T_1-T_2) Thermocouple

Note: (1) EMF is given in absolute millivolt.

(2) Reference junction is at 0°C.

(3) Temperature is in absolute scale.

Temperature (°K)	EMF (mV)	Temperature (°K)	EMF (mV)
74	6.17	95	5.78
75	6.15	96	5.76
76	6.14	97	5.74
77	6.12	98	5.72
78	6.11	99	5.70
79	6.09	100	5.68
80	6.07	101	5.65
81	6.06	102	5.63
82	6.04	103	5.61
83	6.02	104	5.58
84	6.00	105	5.56
85	5.99	106	5.54
86	5.97	107	5.51
87	5.95	108	5.49
88	5.92	109	5.46
89	5.91	110	5.44
90	5.88	111	5.42
91	5.86	112	5.39
92	5.84	113	5.37
93	5.82	114	5.34
94	5.80	115	5.32

Temperature (°K)	EMF (mV)	Temperature (°K)	EMF (mV)
116	5.30	142	4.61
117	5.27	143	4.58
118	5.25	144	4.55
119	5.22	145	4.52
120	5.20	146	4.50
121	5.17	147	4.47
122	5.15	148	4.43
123	5.12	149	4.41
124	5.10	150	4.38
125	5.07	151	4.35
126	5.05	152	4.31
127	5.02	153	4.29
128	5.00	154	4.26
129	4.97	155	4.23
130	4.94	156	4.20
131	4.92	157	4.17
132	4.89	158	4.14
133	4.86	159	4.11
134	4.83	160	4.07
135	4.81	161	4.04
136	4.77	162	4.01
137	4.75	163	3.98
138	4.72	164	3.95
139	4.69	165	3.92
140	4.66	166	3.89
141	4.64	167	3.86

Temperature (°K)	EMF (mV)	Temperature (°K)	EMF (mV)
168	3.83	194	2.97
169	3.80	195	2.94
170	3.77	196	2.90
171	3.74	197	2.86
172	3.70	198	2.83
173	3.67	199	2.80
174	3.69	200	2.76
175	3.60	201	2.72
176	3.57	202	2.68
177	3.54	203	2.65
178	3.51	204	2.62
179	3.48	205	2.58
180	3.44	206	2.54
181	3.41	207	2.50
182	3.38	208	2.47
183	3.35	209	2.44
184	3.32	210	2.40
185	3.28	211	2.36
186	3.24	212	2.32
187	3.21	213	2.29
188	3.18	214	2.26
189	3.14	215	2.22
190	3.10	216	2.18
191	3.07	217	2.14
192	3.04	218	2.11
193	3.00	219	2.08

Temperature (°K)	EMF (mV)
220	2.04
221	2.00
222	1.97
223	1.93
224	1.89
225	1.85
226	1.82
227	1.78
228	1.74
229	1.70
230	1.67
231	1.63
232	1.59
233	1.55
234	1.52
235	1.48
236	1.44
237	1.40
238	1.37
239	1.33
240	1.29

APPENDIX III

Magnetoconductivity in the Quantum Limit

The force equation of the electrons of the effective mass m*, charge e, and velocity v in an electric field E and magnetic field H is

$$m^* \left(\frac{d\underline{v}}{dt} + \frac{\underline{v}}{\tau}\right) = -e\,(\underline{E} + \underline{v} \times \underline{H}) \qquad (1)$$

where τ is the relaxation time of the electrons. If the magnetic field is along the Z-axis, then

$$\underline{v} \times \underline{H} = \begin{vmatrix} i & j & k \\ v_x & v_y & v_z \\ o & o & H \end{vmatrix}$$

Since for a spherical energy surface, the cyclotron angular frequency of electrons, w, is given by

$$w = \frac{eH}{m^*}$$

In steady state, $\frac{dv}{dt} = o$

Equation (1) in component forms becomes

$$v_x = -\frac{e\tau}{m^*} E_x - w\tau v_y$$

$$v_y = -\frac{e\tau}{m^*} E_y + w\tau v_x$$

or

$$v_x = -\frac{e}{m^*}\left(\frac{\tau}{1+w^2\tau^2} E_x - \frac{w\tau^2}{1+w^2\tau^2} E_y\right)$$

$$v_y = -\frac{e}{m^*}\left(\frac{\tau}{1+w^2\tau^2} E_y + \frac{w\tau^2}{1+w^2\tau^2} E_x\right)$$

Since all the electrons do not have the same value of τ, angular brackets can be used in the expression to represent the statistical average and

$$J_x = \frac{ne^2}{m^*} \left(\left\langle \frac{\tau}{1+w^2\tau^2} \right\rangle E_x - \left\langle \frac{w\tau^2}{1+w^2\tau^2} \right\rangle E_y \right)$$

$$J_y = \frac{ne^2}{m^*} \left(\left\langle \frac{w\tau^2}{1+w^2\tau^2} \right\rangle E_x + \left\langle \frac{\tau}{1+w^2\tau^2} \right\rangle E_y \right)$$

Also $J_x = \sigma_{xx} E_x - \sigma_{xy} E_y$

$$J_y = \sigma_{yx} E_x + \sigma_{xx} E_y$$

so that $\sigma_{xx} = \frac{ne^2}{m^*} \left\langle \frac{\tau}{1+w^2\tau^2} \right\rangle$

$$\sigma_{xy} = -\sigma_{yx} = \frac{ne^2}{m^*} \left\langle \frac{w\tau^2}{1+w^2\tau^2} \right\rangle$$

From equation (4.1.15)

$$\sigma_1 = \frac{(\Sigma\sigma_{xx})^2 + (\Sigma\sigma_{xy})^2}{\Sigma\sigma_{xx}}$$

$$= \frac{(\sigma_{cxx} + \sigma_{ixx})^2 + (\sigma_{cxy} + \sigma_{ixy})^2}{\sigma_{cxx} + \sigma_{ixx}}$$

If (i) $\sigma_{cxy} \gg \sigma_{cxx} + \sigma_{ixx}$

(ii) $\sigma_{cxy} \gg \sigma_{ixy}$

(iii) $\sigma_{cxx} \gg \sigma_{ixx}$

It reduces to the case of electrical conduction in a single band and

$$\sigma_{\perp} \longrightarrow \frac{\sigma_{cxy}^2}{\sigma_{cxx}}$$

$$\longrightarrow \frac{\left[\frac{ne^2}{m^*} < \frac{w\tau^2}{1+w^2\tau^2} > \right]^2}{\frac{ne^2}{m^*} < \frac{\tau}{1+w^2\tau^2} >}$$

$$\longrightarrow \frac{ne^2}{m^*} <\tau> < \frac{w^2\tau^2}{1+w^2\tau^2} >$$

But mobility of the electron is independent of the magnetic field and temperature in the longitudinal configuration, and

$$\sigma_{\parallel} = n\,e\,u = \frac{ne^2<\tau>}{m^*}$$

Therefore $\sigma_{\perp} \longrightarrow \sigma_{\parallel} < \frac{w^2\tau^2}{1+w^2\tau^2} >$

Since $w\tau \gg 1$

Therefore $\sigma_{\perp} \longrightarrow \sigma_{\parallel}$ in the high magnetic field limit.

REFERENCES

1969

H1 P.E. Henley, E.H. Rhoderick, J.Phys.Co., Proc.Phys.Soc. (Solid State Physics), Ser. 2, Vol. 2, No. 2, pp.365-71.

L1 D.M. Larson, J.Phys. Chem. Solids 29, 271.

1968

D1 J. Durkan, R.J. Elliott, N.H. March, Rev.Mod.Phys. 40, 812.

P1 R.V. Parfen'ev, I.I. Farbshtein and S.S. Shalyt, Soviet Phys. JEPT, 26, 906.

1967

A1 Ya. Agaev, O. Mosanov and O. Ismailov, Fizika i Tekhnika Polyprovodnikov, Vol. 1, No. 8, pp.1169-1173.

B1 R.I. Bashirov, M.M. Gadzhialiev, Soviet Phys. Semiconductors 2, 96.

B2 O. Beckman, E. Manamura, N.J. Neuringer, Physical Review Letters 18, 773.

F1 F.W. Fenton, R.R. Haering, Phys.Rev. 159, 593.

M1 H. Miyazawa, H. Ikoma, Journ.Phys.Soc., Japan, Japan 23, 290.

1966

D1 I.L. Drichko, I.V. Mochan, Soviet Physics - Solid State, Vol. 7, 2634.

K1 V.A. Kudinov, B.Ya. Moizhes, Soviet Physics - Solid State, Vol. 7, 1868.

M1 V.M. Muzhdaba, R.V. Parfen'ev, S.S. Shalyt, Soviet Phys. Solid State 7, 1922.

P1 S.M. Puri, T.H. Geballe, Semiconductors and Semi-metals, Vol. 1 Eds. R.K. Willardson and A.C. Beer (New York: Academic Press).

P2 E.H. Putley, Semiconductors and Semi-metals, Vol. 1, Eds. R.K. Willardson and A.C. Beer (New York: Academic Press).

1965

K1 R. Kubo, S.J. Miyake, N. Hashitsume, Solid State Physics, Vol. 17, Eds. F. Seitz and D. Turnbull (New York: Academic Press).

M1 V.M. Muzhdaba, S.S. Shalyt, R.V. Parfen'ev, Soviet Phys. Solid State 6, 2554.

S1 S.S. Shalyt, V.M. Muzhdaba, R.V. Parfen'ev, Soviet Phys. JEPT 20, 294.

T1 I.M. Tsidil'kovskii, M.M. Aksel'rod, V.I. Sokolov, Soviet Phys. Solid State 7, 253.

1964

F1 Yu.A. Firsov, V.L. Gurevich, R.V. Parfen'ev, S.S. Shalyt, Physical Review Letters 12, 660.

M1 S.C. Miller, Phys.Rev. 133, A1138.

P1 R.J. Phelan, Jr, W.F. Love, Phys.Rev. 133, A1134.

S1 S.S. Shalyt, V.M. Muzhdaba, R.V. Parfen'ev, Soviet Phys. Solid State 6, 508.

1963

G1 V.L. Gurevich, Yu.A. Firsov, A.L. Efros, Soviet Phys. Solid State 4, 1331.

P1 S.M. Puri, T.H. Geballe, Bull.Am.Phys.Soc. 8, no. 4, 309.

1962

E1 A.L. Efros, Soviet Phys. Solid State 3, 2079.

F1 Yu.A. Firsov, V.L. Gurevich, Soviet Phys. JEPT 14, 367.

H1 M. Hass and W. Henvis, J.Phys.Chem. Solids 23, 1099.

K1 R.F. Kazarinov and V.G. Skobov, Soviet Phys. JEPT 15, 726.

T1 I.M. Tsidil'kovskii, Thermomagnetic effects in semiconductors, Inforesearch, Ltd., London.

1961

G1 V.L. Gurevich, Yu.A. Firsov, Soviet Phys. JEPT 13, 137.

P1 E.D. Palik, G.S. Teitler, G.S. Pikus and R.F. Wallis, Phys.Rev. 122, 475.

1960

H1 C. Herring, J.Appl.Phys. 31, 1939.

N1 D.N. Nasledov, Lien Chich-ch'ao, Soviet Phys. Solid State 2, 729.

P1 E.H. Puttley, Proc.Phys.Soc. (London) 76, 802.

1959

A1 E.N. Adams and T.D. Holstein, J.Phys.Chem. Solids 10, 254-276.

B1 R. Bate, R.R. Willardson, A.C. Beer, J.Phys.Chem. Solids 9, 119.

E1 H. Ehrenreich, J.Phys.Chem. Solids, 9, 129.

P1 E.H. Putley, Proc.Phys.Soc. 73, 280.

1958

S1 R.J. Sladek, J.Phys.Chem. Solids 5, 157.

1956

K1 R.W. Keyes, R.J. Sladek, J.Phys.Chem. Solids 1, 143.

M1 R. Mansfield, Proc.Phys.Soc. 69, 76.

Y1 Y. Yafet, R.W. Keyes and E.N. Adams, J.Phys.Chem. Solids 1, 137

1955

F1 H. Fritzsche, Phys.Rev. 99, 406.

1954

M1 W.H. Mitchell, J.Sci.Instrum. 31, 147.

1951

G1 R. Gilmount, Analytical Chem. 23, 157.

1950

H1 C.S. Hung, Phys.Rev. 79, 729.

1930

L1 L. Landau, Z.Physik 64, 629.

1928

G1 W. Gerlach, Handb. d. Phys. 13, 228 (Berlin: Springer).

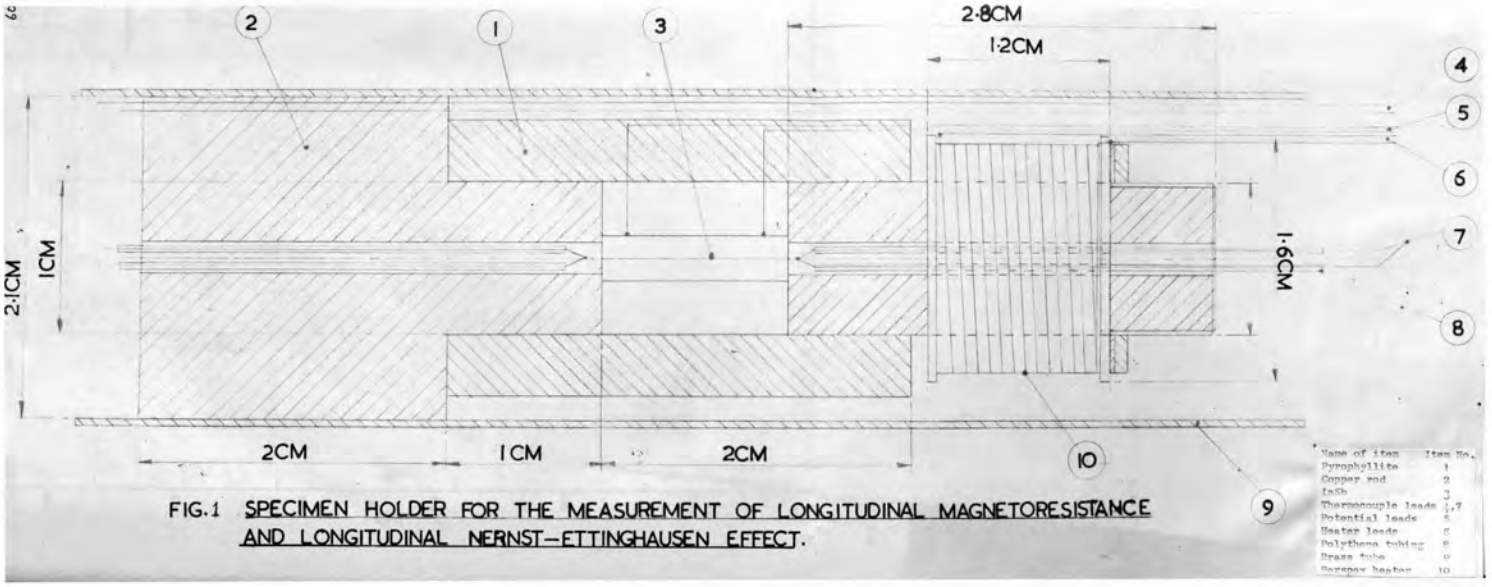

FIG.1 SPECIMEN HOLDER FOR THE MEASUREMENT OF LONGITUDINAL MAGNETORESISTANCE AND LONGITUDINAL NERNST–ETTINGHAUSEN EFFECT.

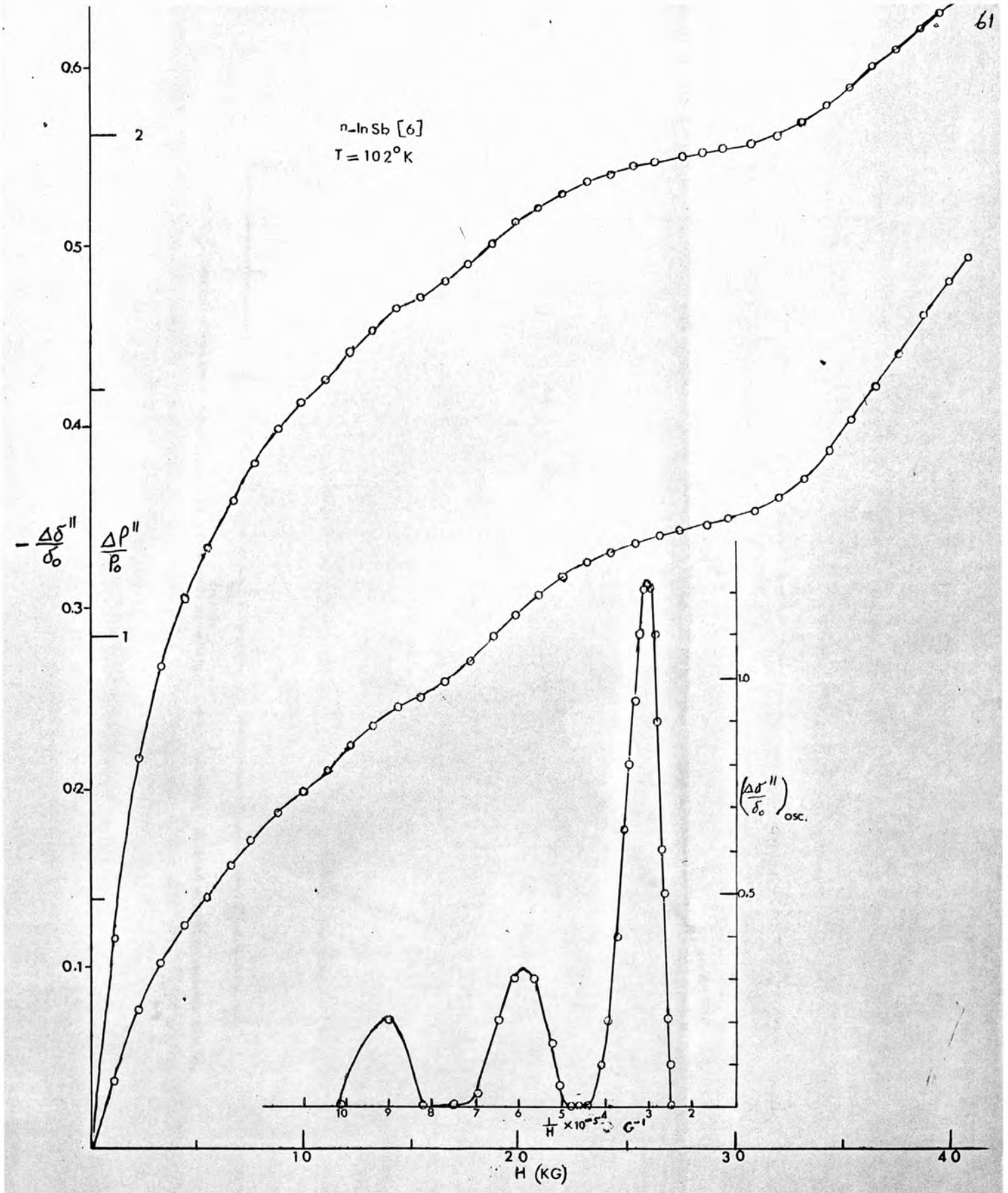

FIG. 2 Gurevich-Firsov oscillations of longitudinal magnetoconductivity

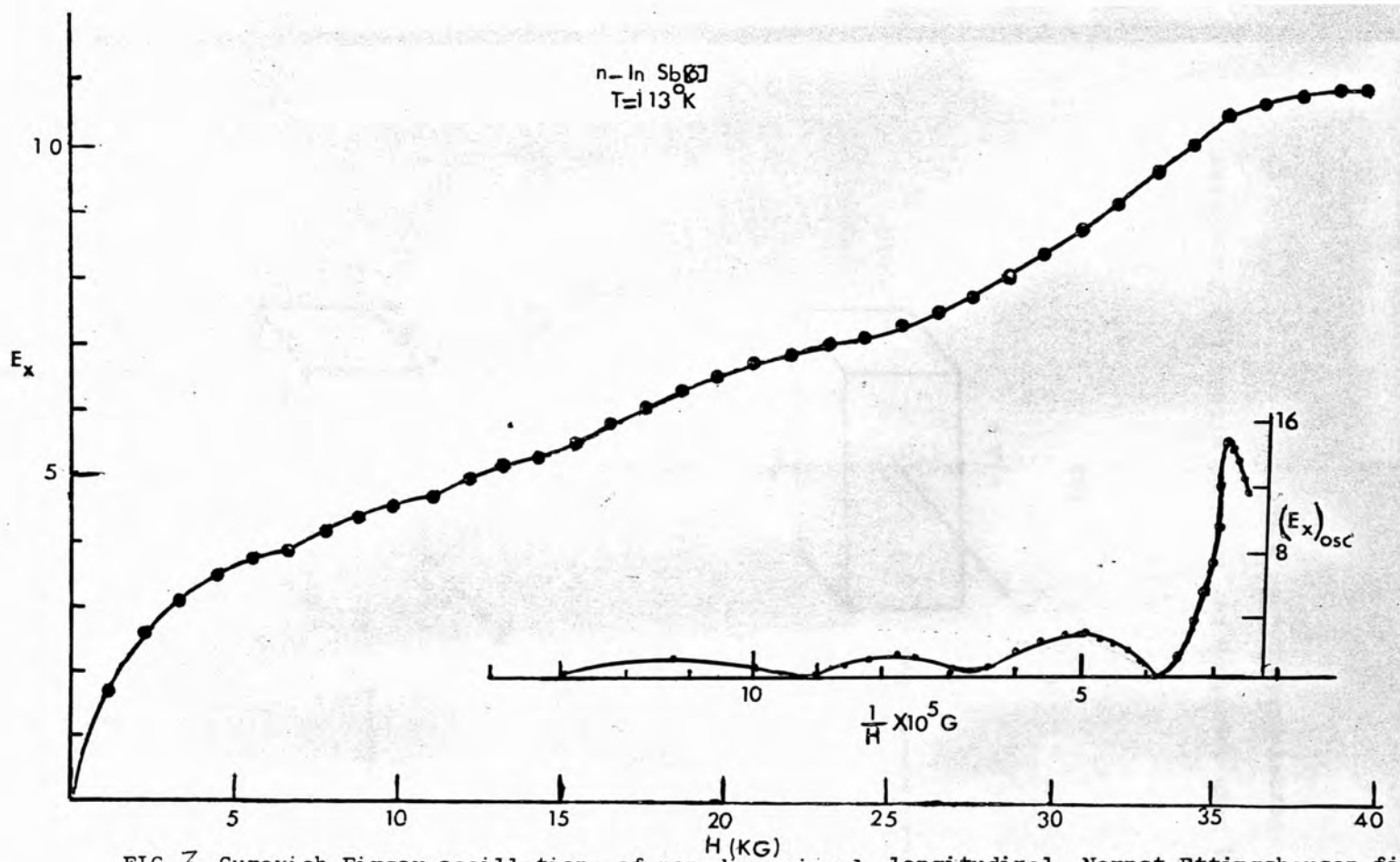

FIG. 3 Gurevich-Firsov oscillations of non-dimensional longitudinal Nernst-Ettingshausen field.

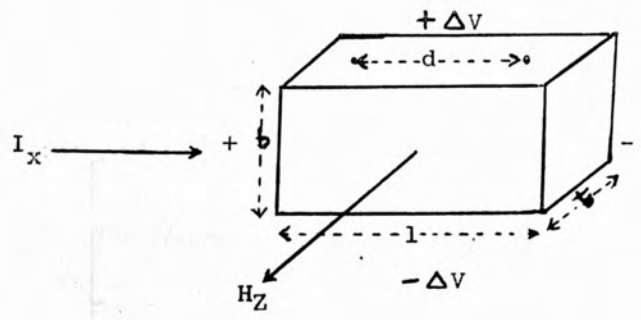

(a)

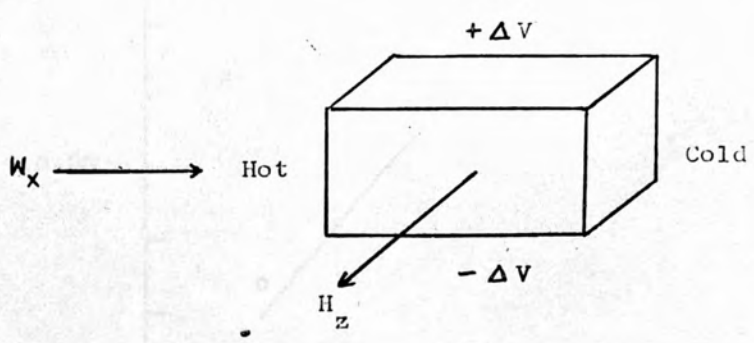

(b)

Fig.4 Sign covention for (a) Hall effect (b) Transverse Nernst-Ettinghausen effect.

$$\text{Correction Factor} = \frac{\text{E.M.F. by standard chromel-alumel thermocouple}}{\text{E.M.F. by } T_1 - T_2 \text{ thermocouple}}$$

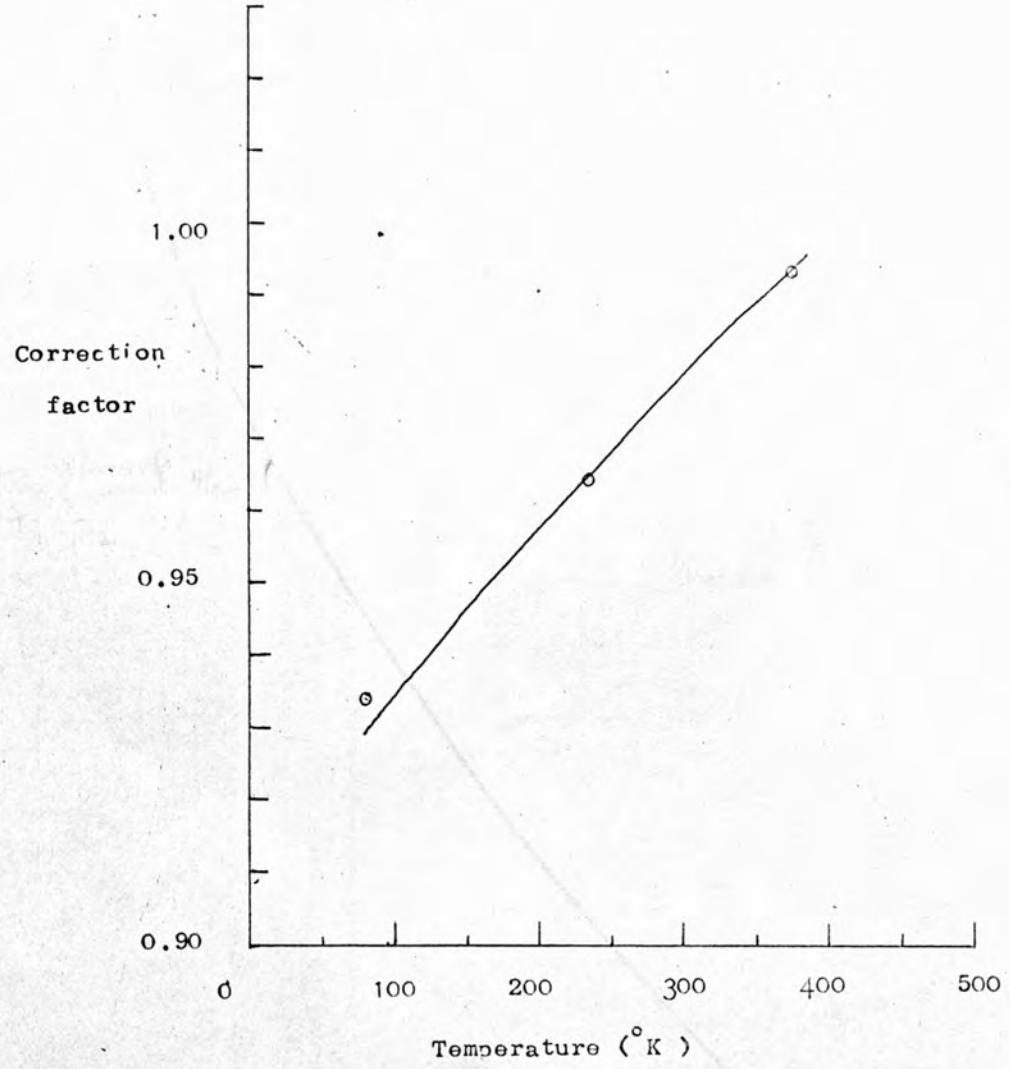

Fig. 5 Correctin curve for $T_1 - T_2$ thermocouple.

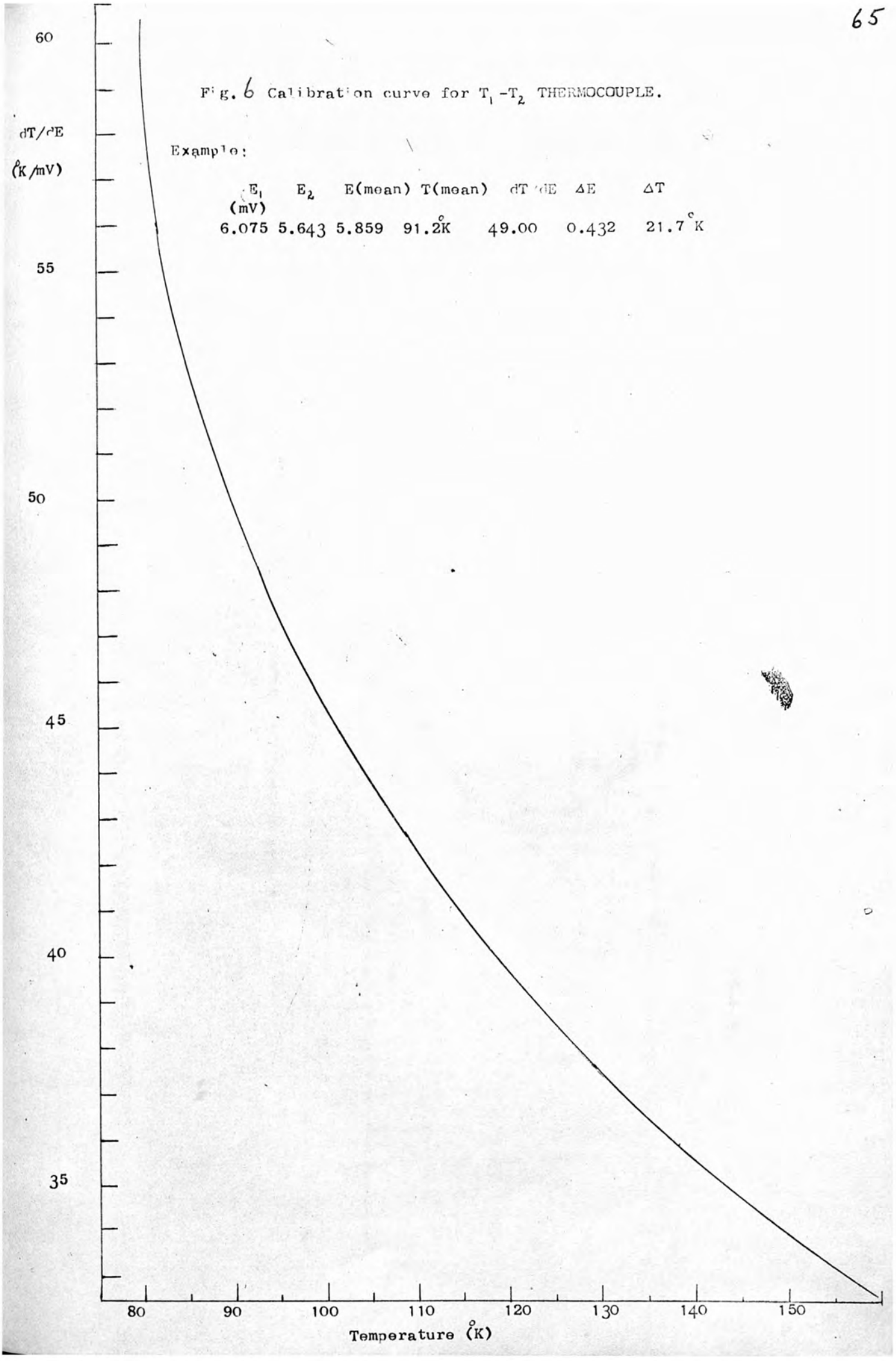

Fig. 6 Calibration curve for $T_1 - T_2$ THERMOCOUPLE.

Example:

E_1 (mV)	E_2	E(mean)	T(mean)	dT/dE	ΔE	ΔT
6.075	5.643	5.859	91.2°K	49.00	0.432	21.7 °K

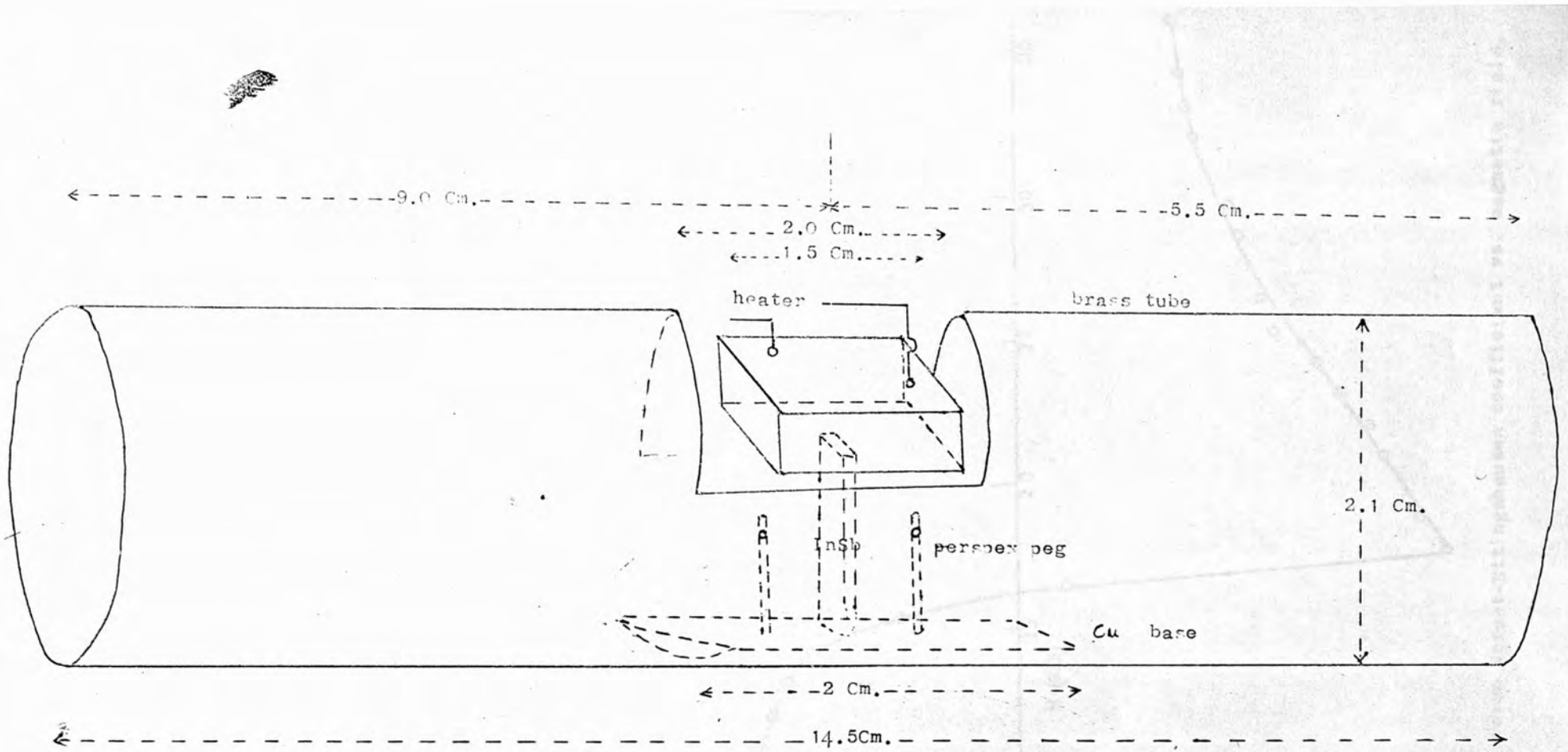

Fig. 7 Specimen holder for the measurement of transverse Nernst Ettinghausen effect.

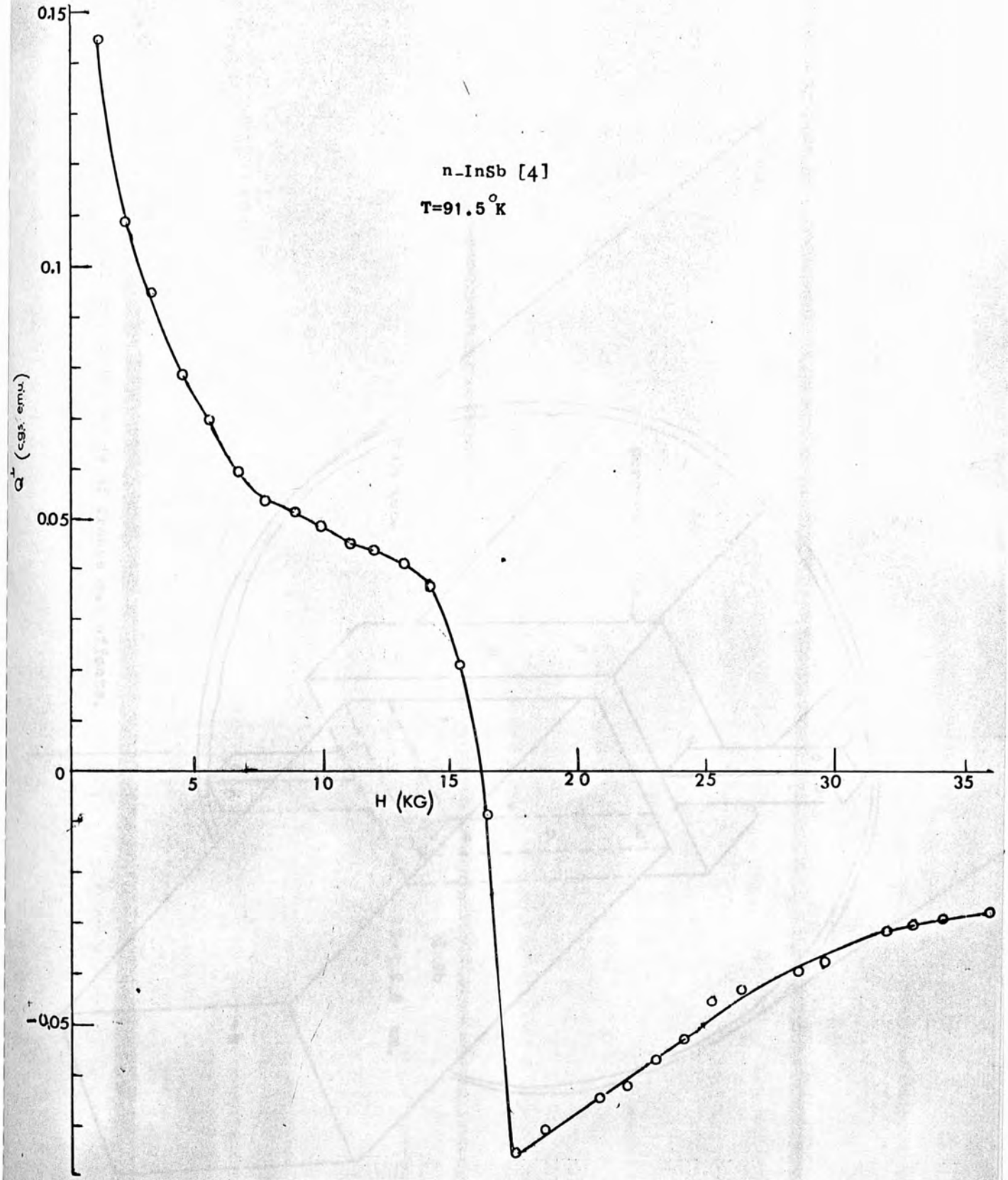

Fig. 8 Transverse Nernst-Ettingshausen coefficient vs. magnetic field.

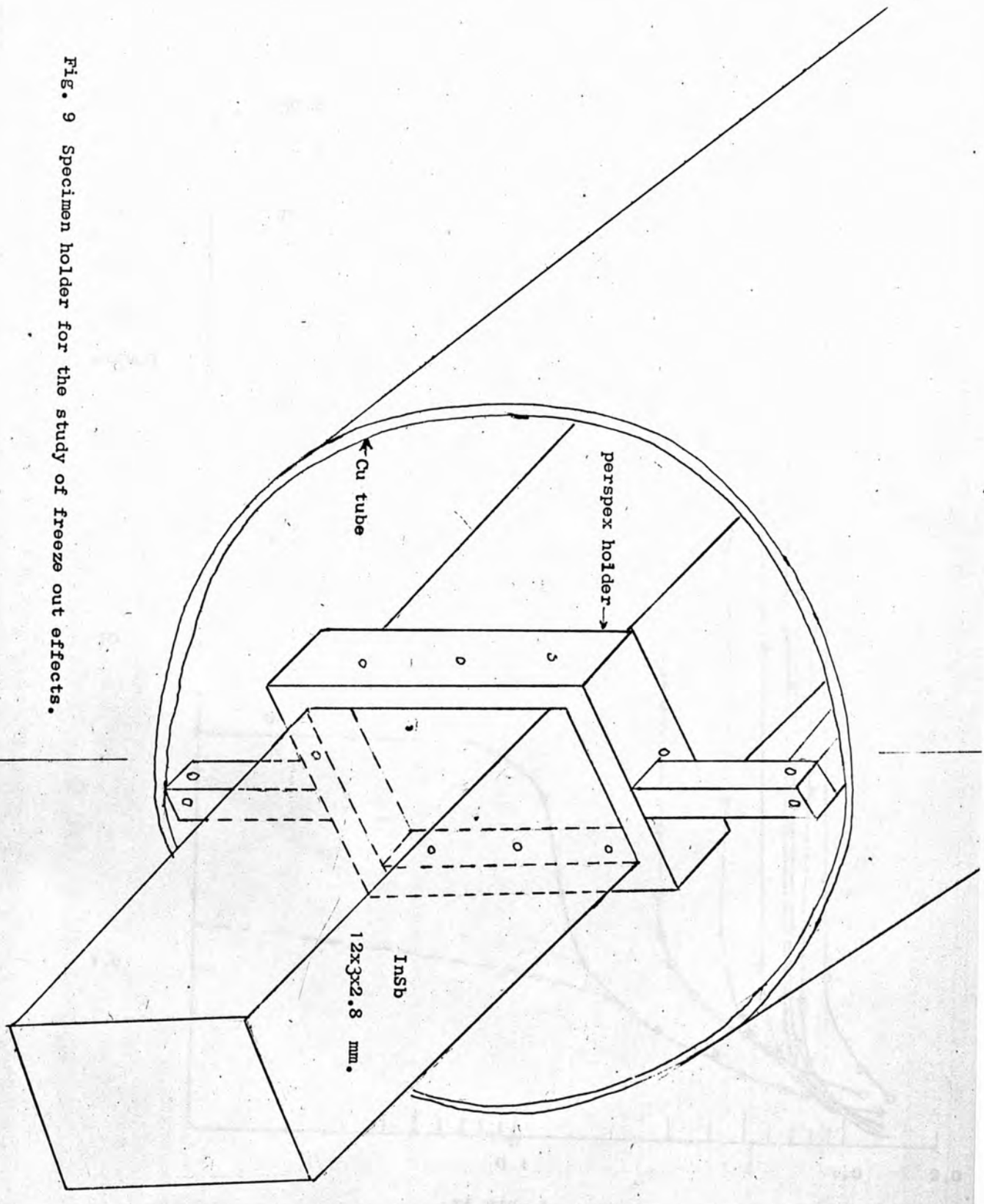

Fig. 9 Specimen holder for the study of freeze out effects.

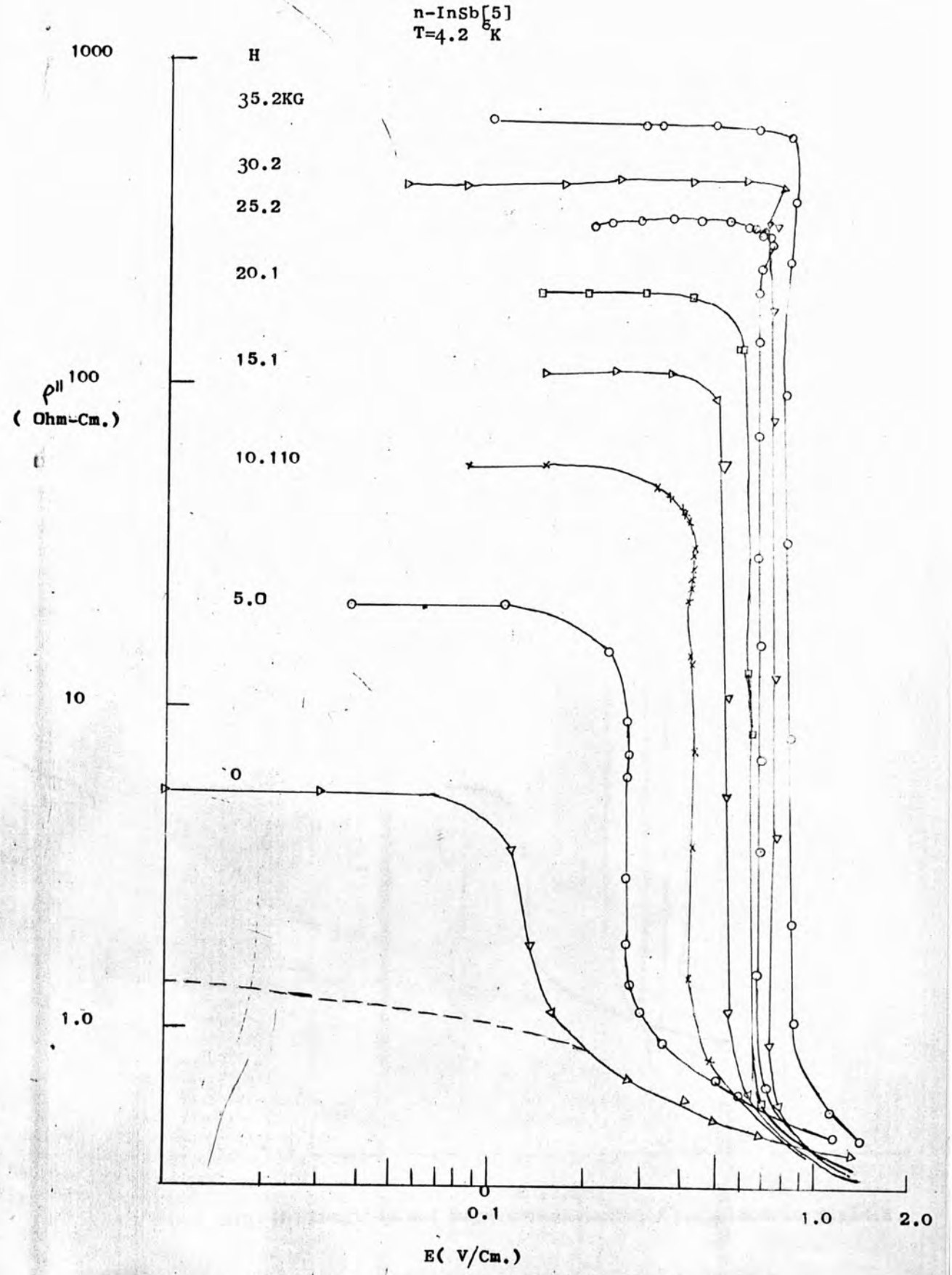

Fig. 10 Longitudinal magnetoresistance, $\rho_{//}$, vs. electric field, E.

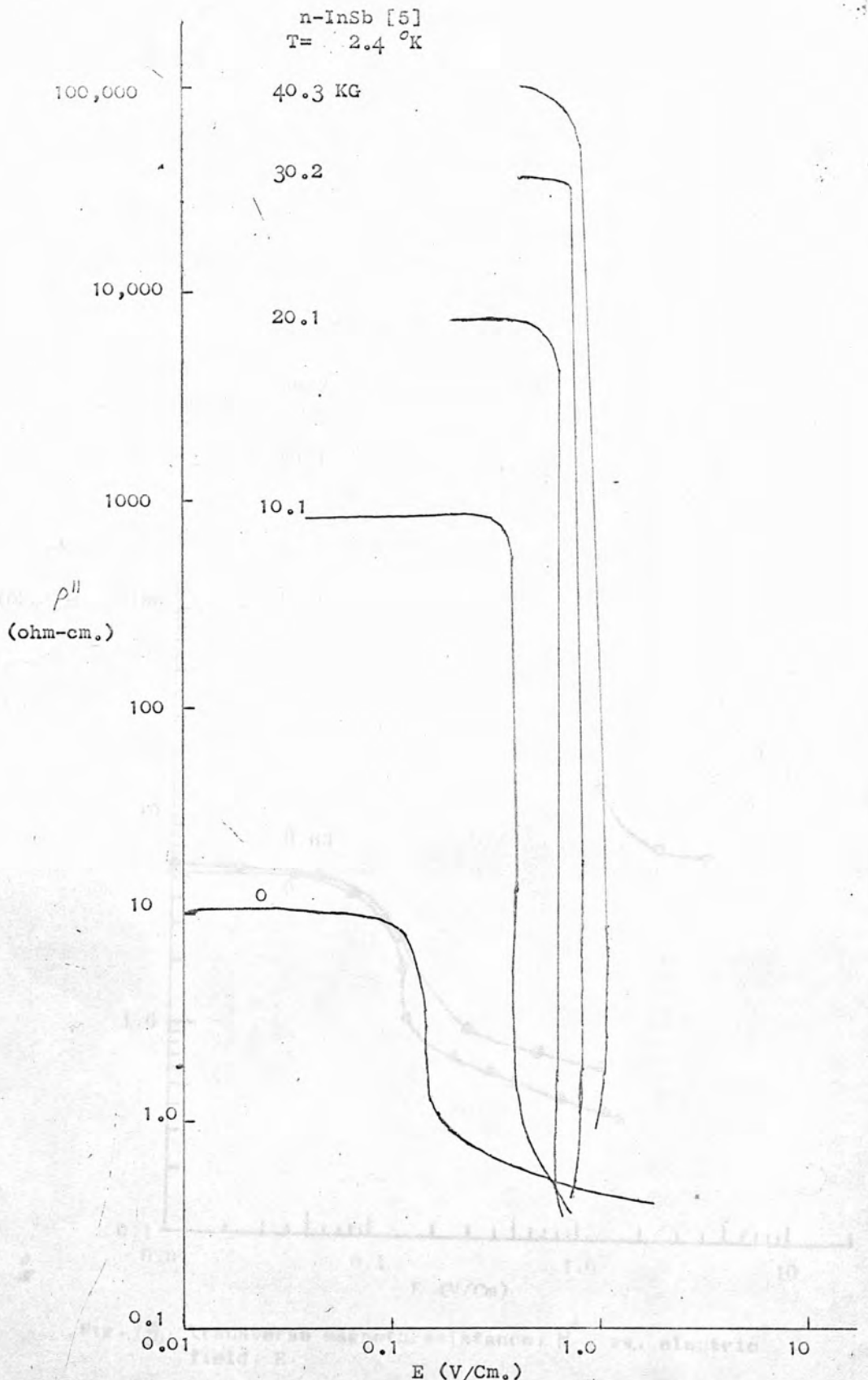

Fig. 11 Longitudinal magnetoresistance, ρ'', vs. electric field, E.

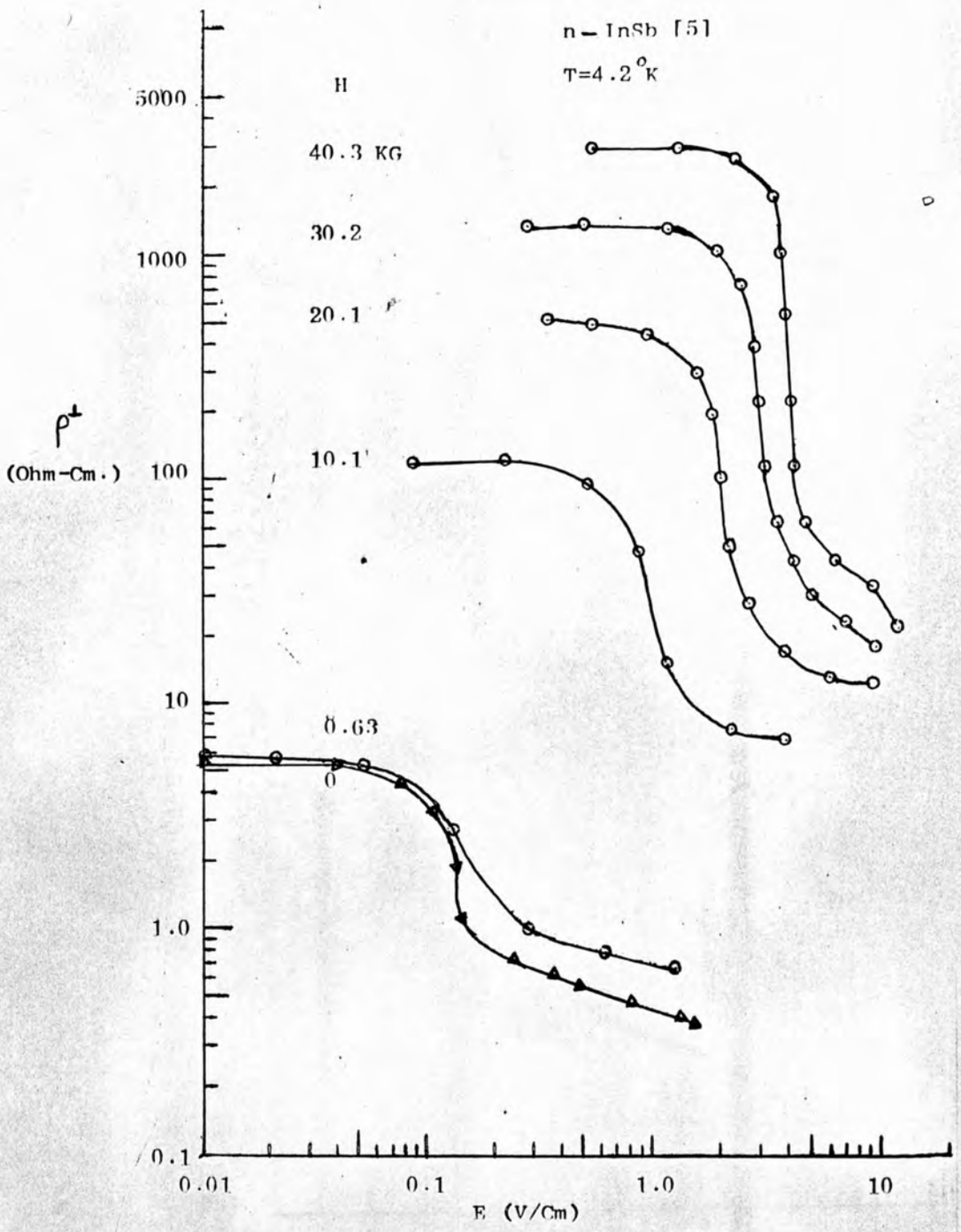

Fig. 12. Transverse magnetoresistance, $\rho^{\perp}$, vs., electric field, E.

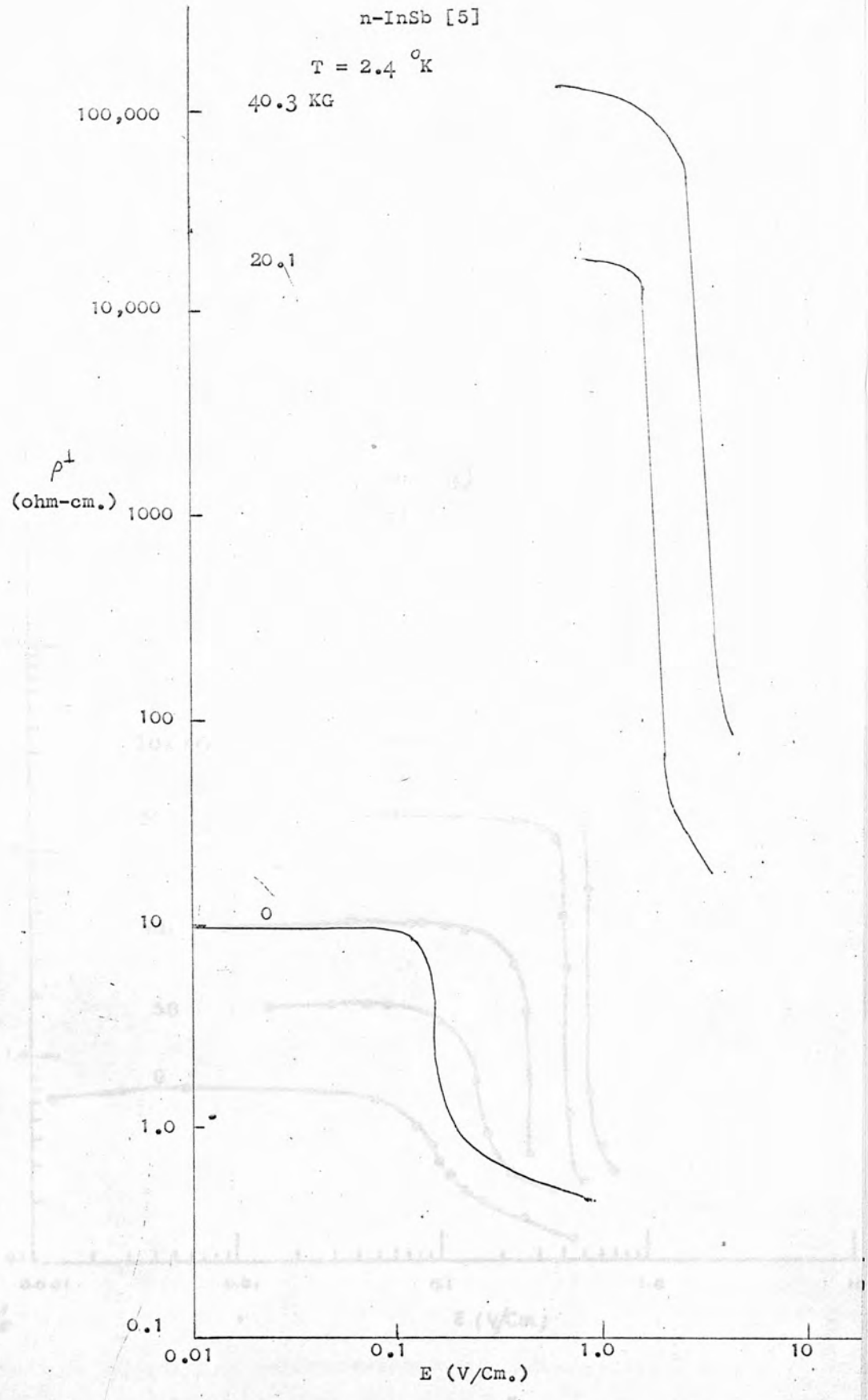

Fig.13 Transverse magnetoresistance, $\rho^{\perp}$, vs. electric field, E.

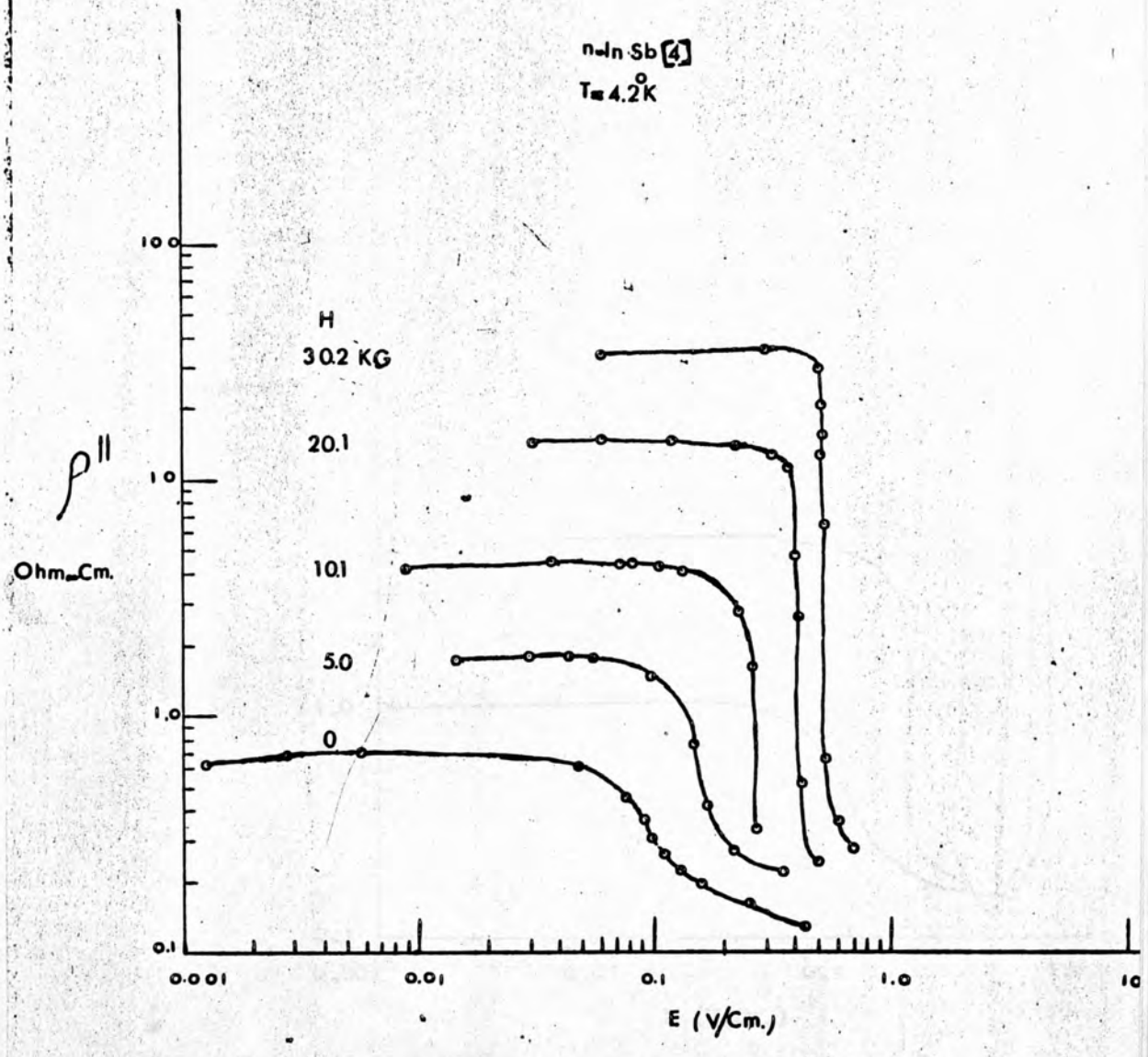

Fig. 14. Longitudinal magnetoresistance, ρ^{N}, vs. electric field, E.

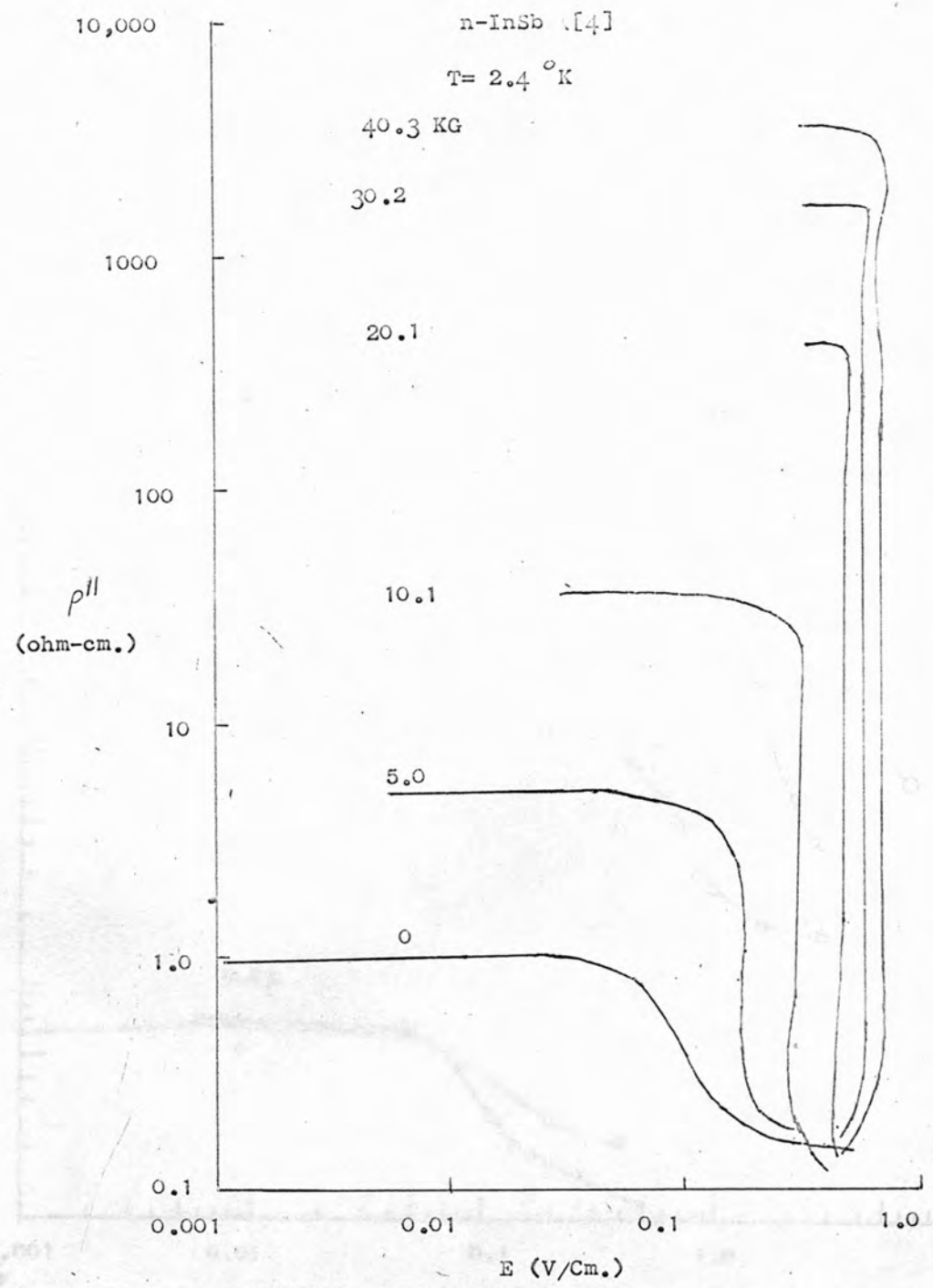

Fig.15 Longitudinal magnetoresistance, ρ'', vs. electric field, E.

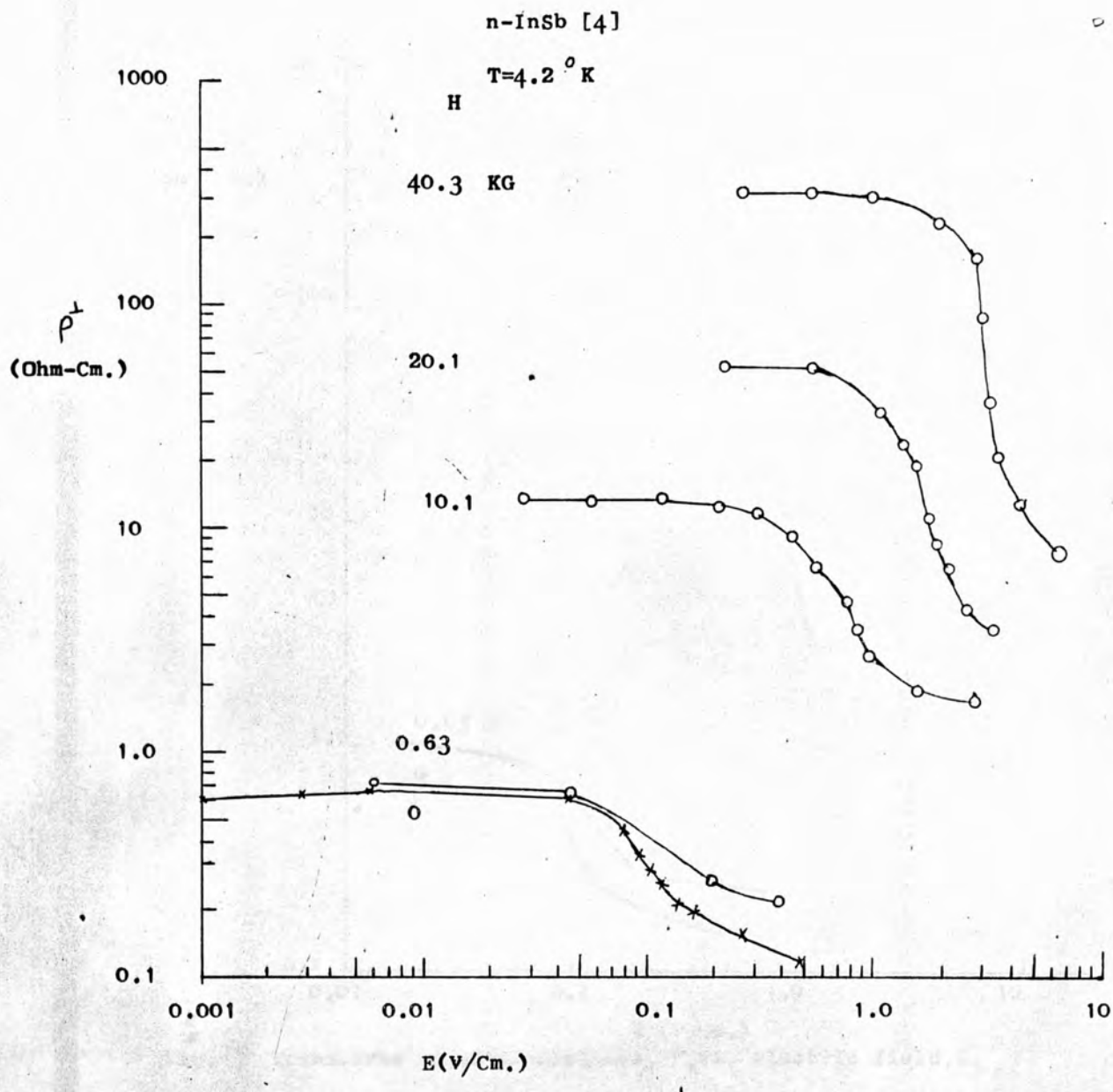

Fig.16 Transverse magnetoresistance , $\rho^{\perp}$, vs.eletric field,E.

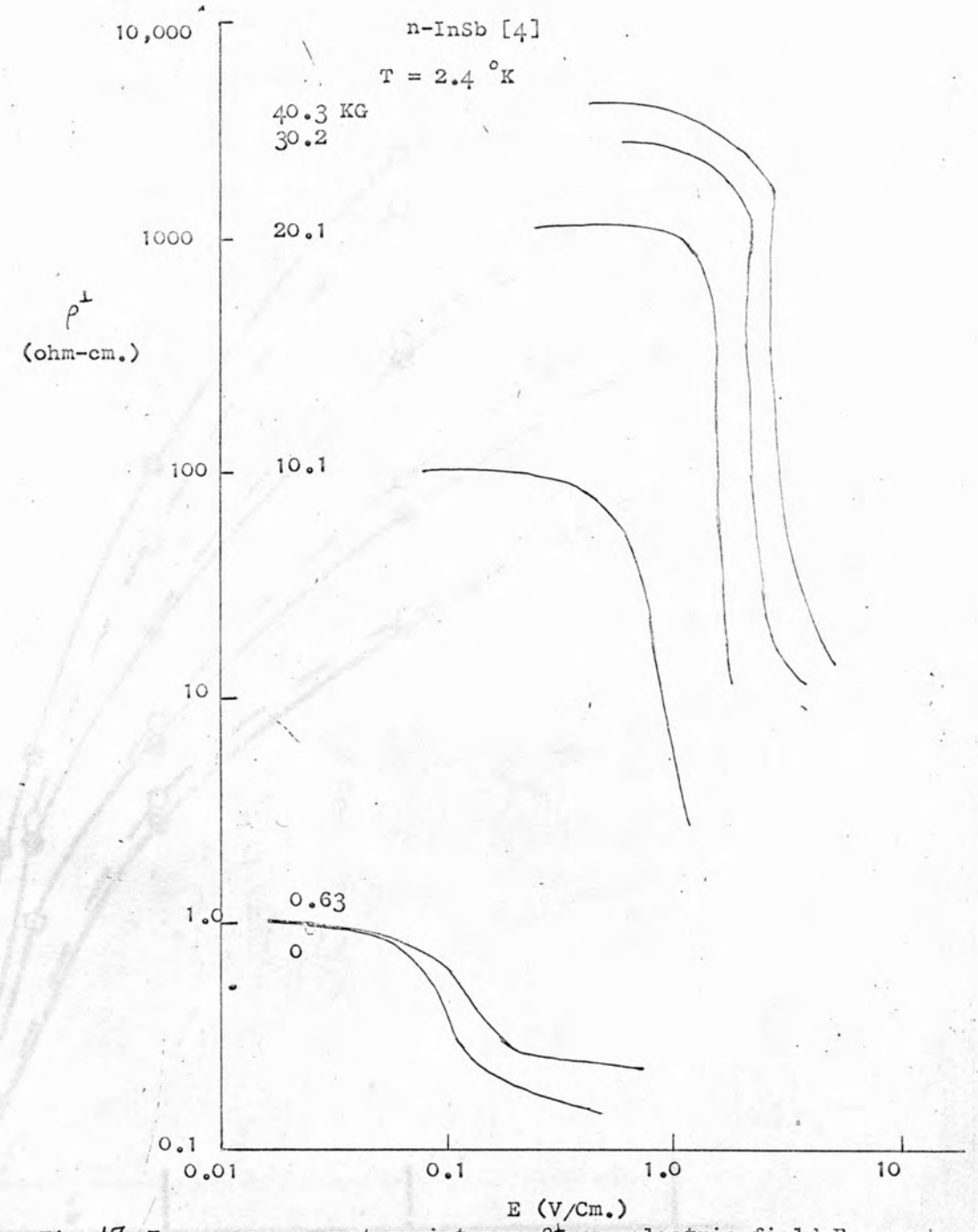

Fig. 17 Transverse magnetoresistance, $\rho^{\perp}$, vs. electric field, E.

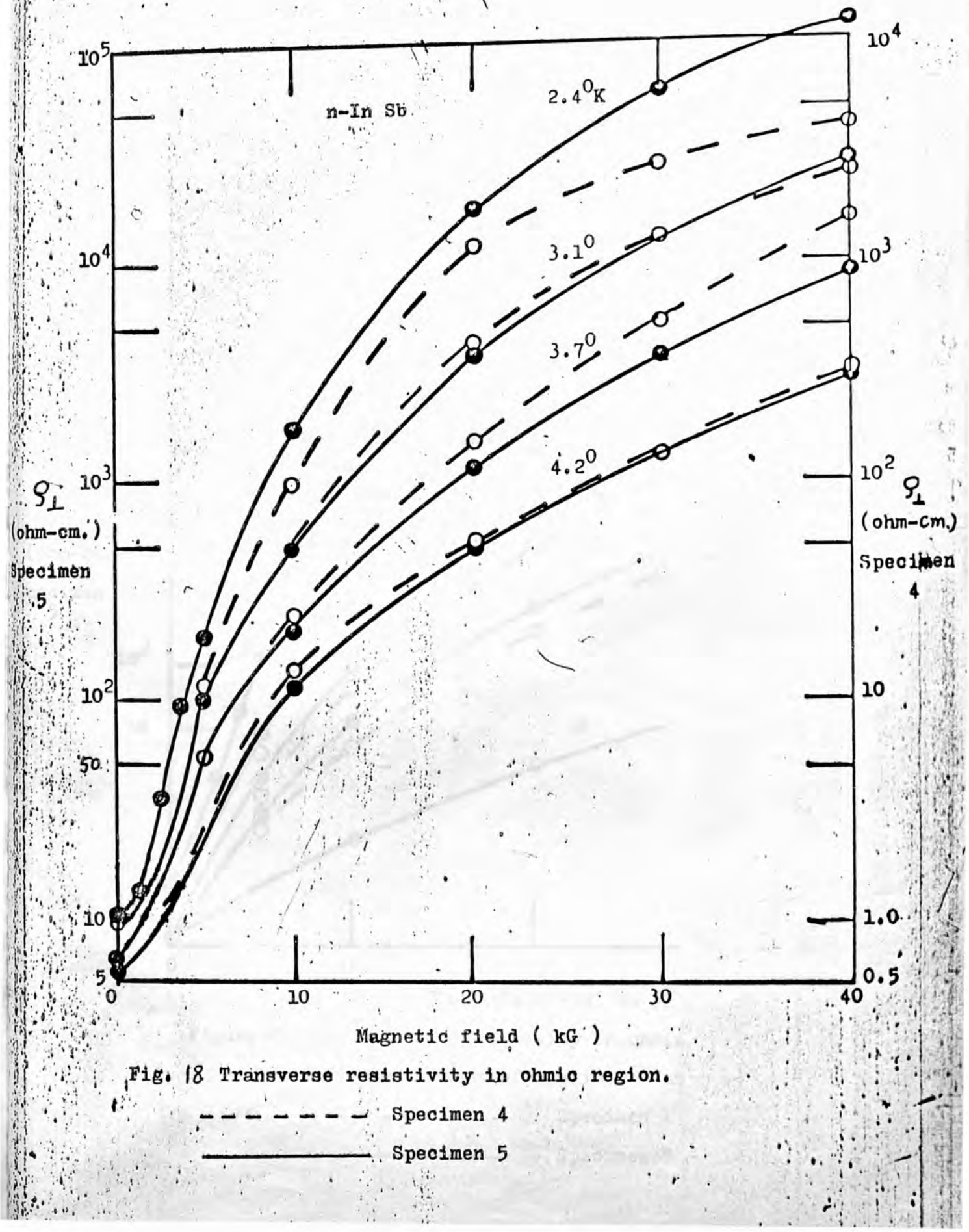

Fig. 18 Transverse resistivity in ohmic region.

– – – – – – Specimen 4

——————— Specimen 5

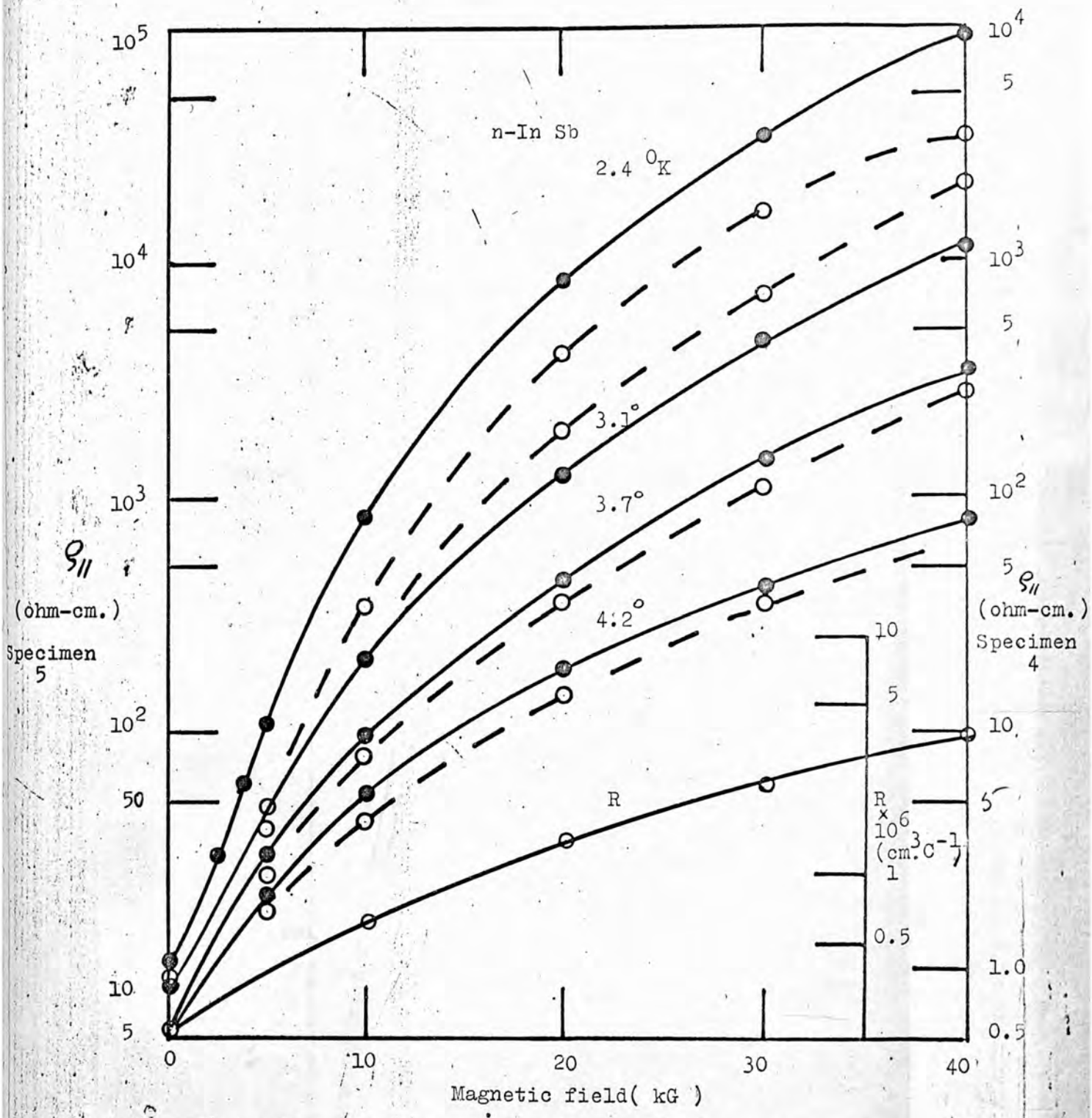

Figure 19 Longitudinal resistivity in ohmic region also Hall coefficient of specimen 5 at 4.2 °K.

– – – – – – – Specimen 4

——————— Specimen 5

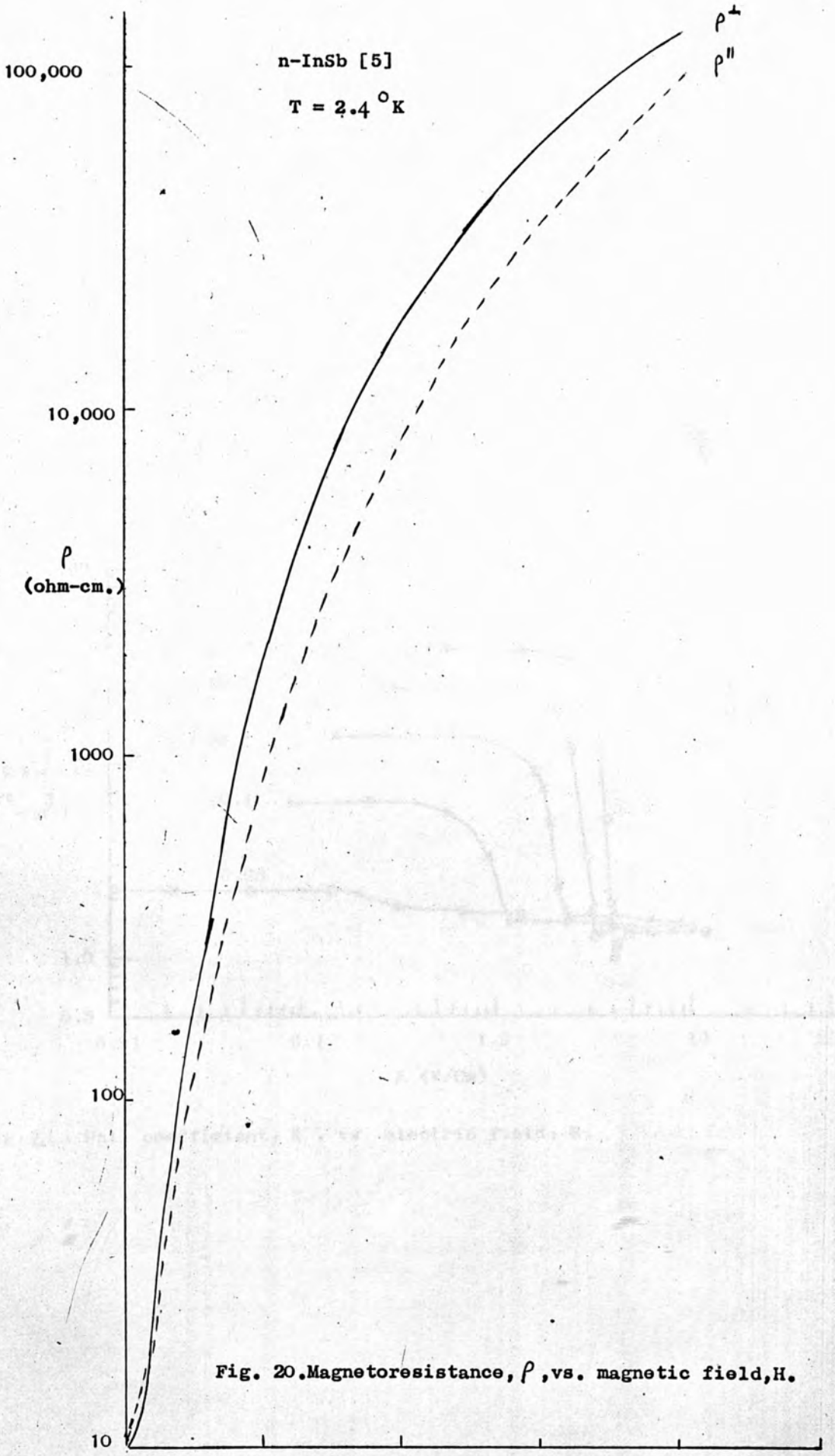

Fig. 20. Magnetoresistance, ρ, vs. magnetic field, H.

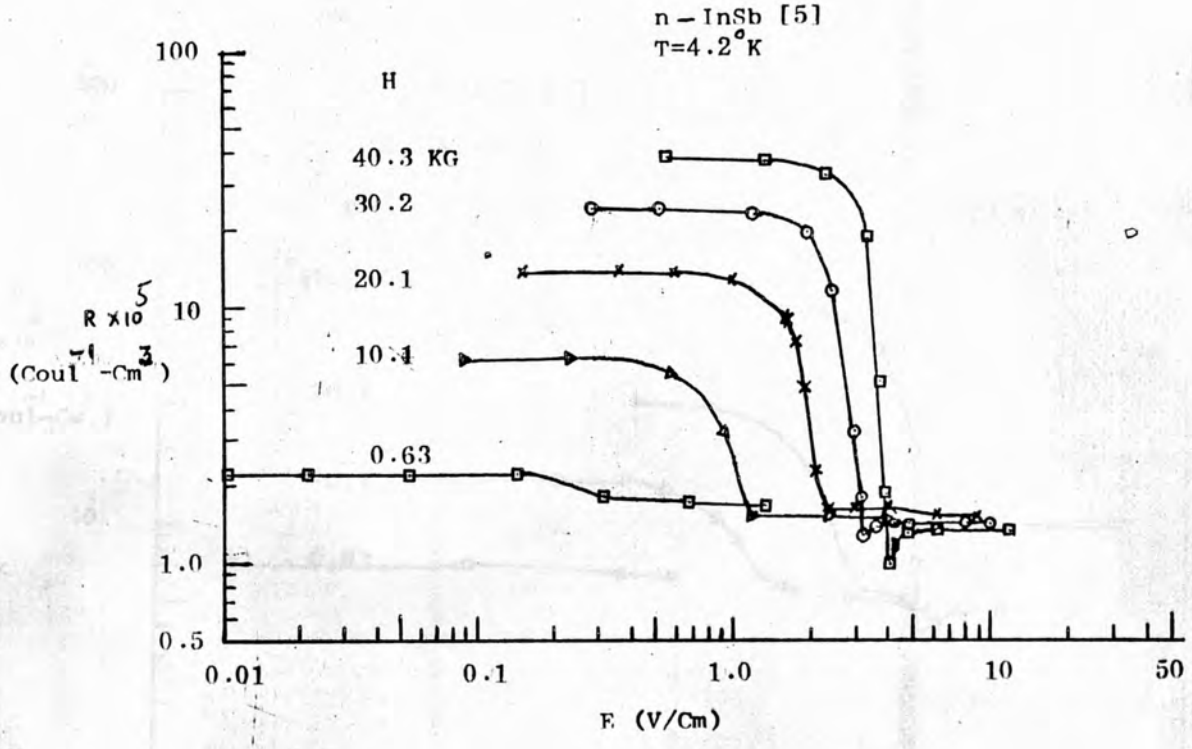

Fig. 21. Hall coefficient, R , vs. electric field, E.

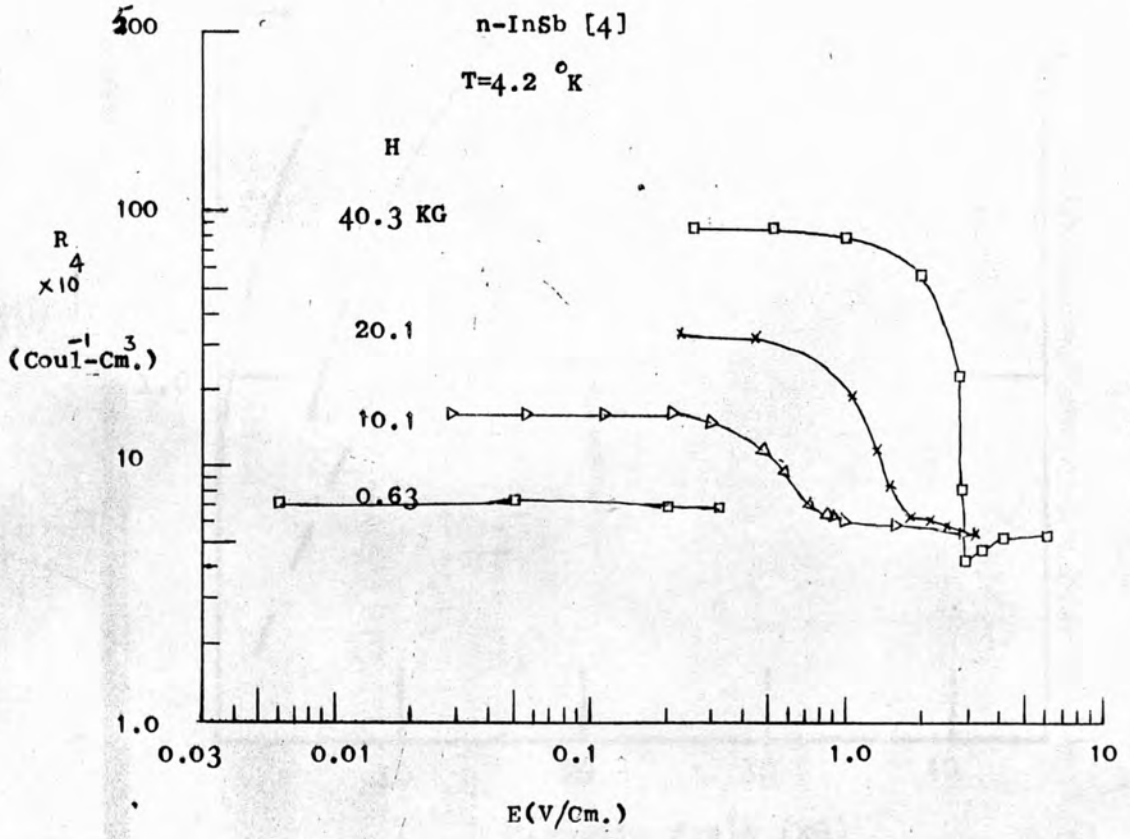

Fig. 22 Hall Coefficient ,R, vs.electric field ,E.

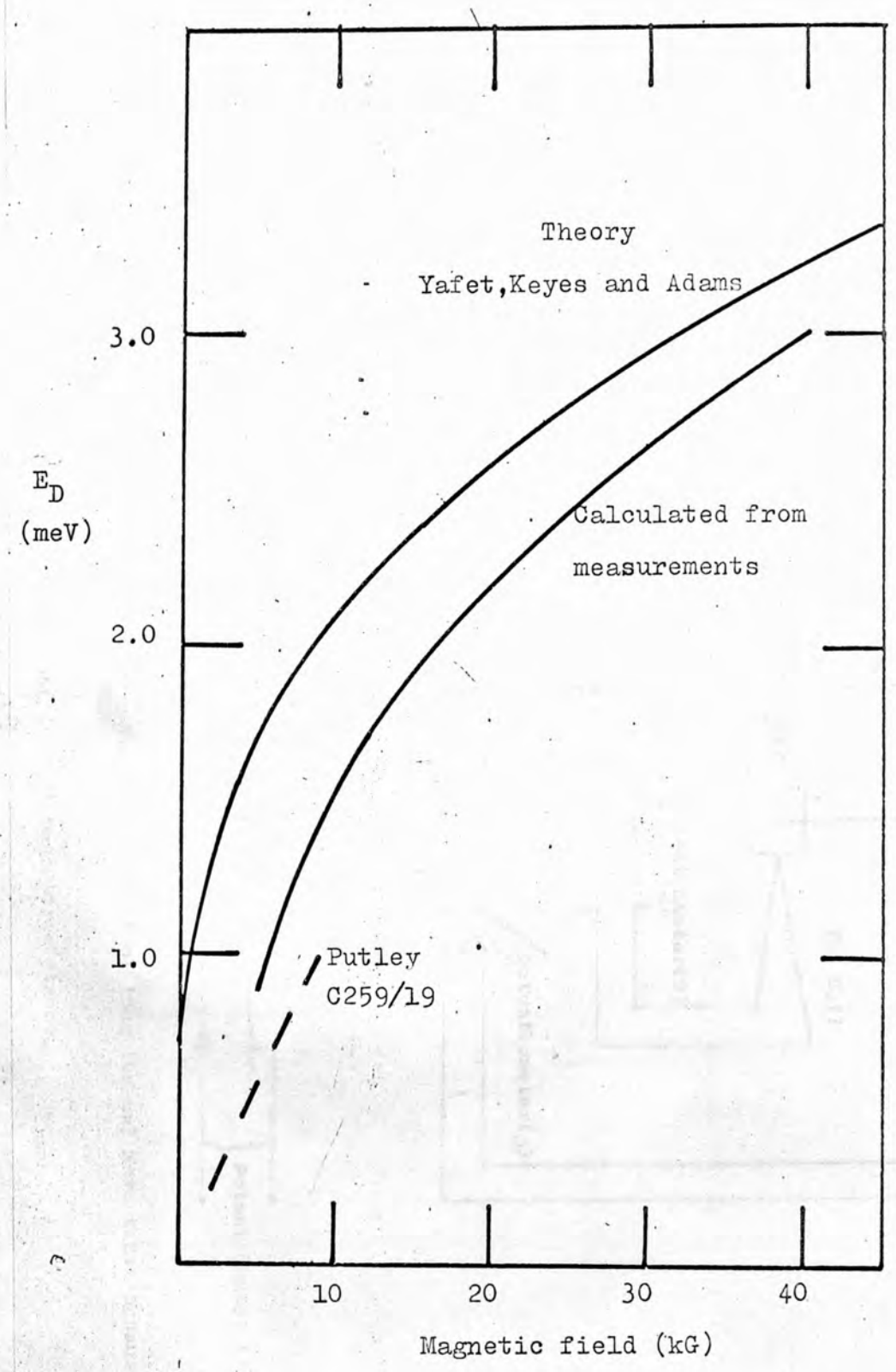

Fig.23. Comparison of theoretical values (assuming $m^*/m = 0.013$, dielectric constant = 16) of the ionization energy of donors E_D with values calculated from the mearsurements. The curve for C259/19 is taken from Putley (1966).

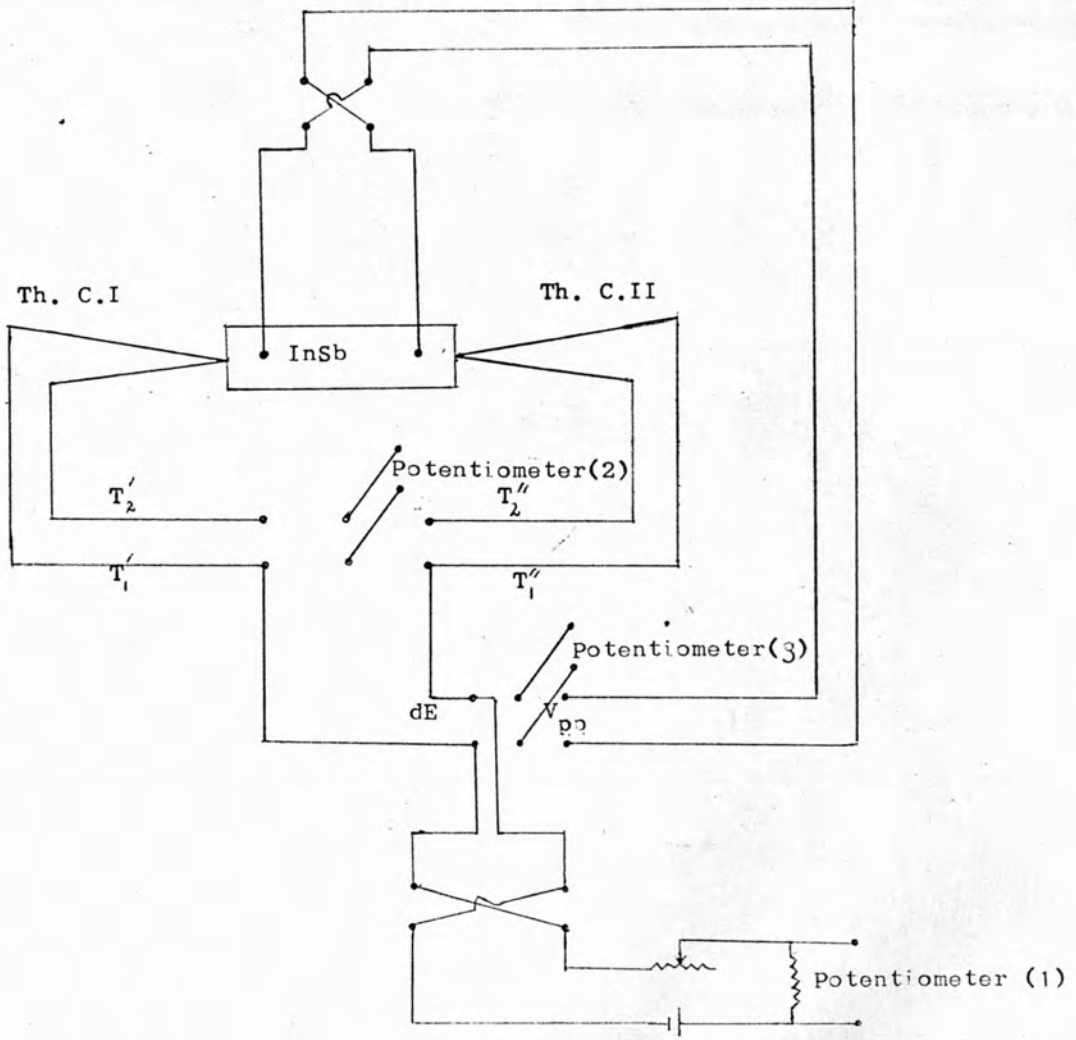

Fig.24 Circuit for the measurement of longitudinal Nernst Ettinghausen effect and longitudinal magnetoresistance.

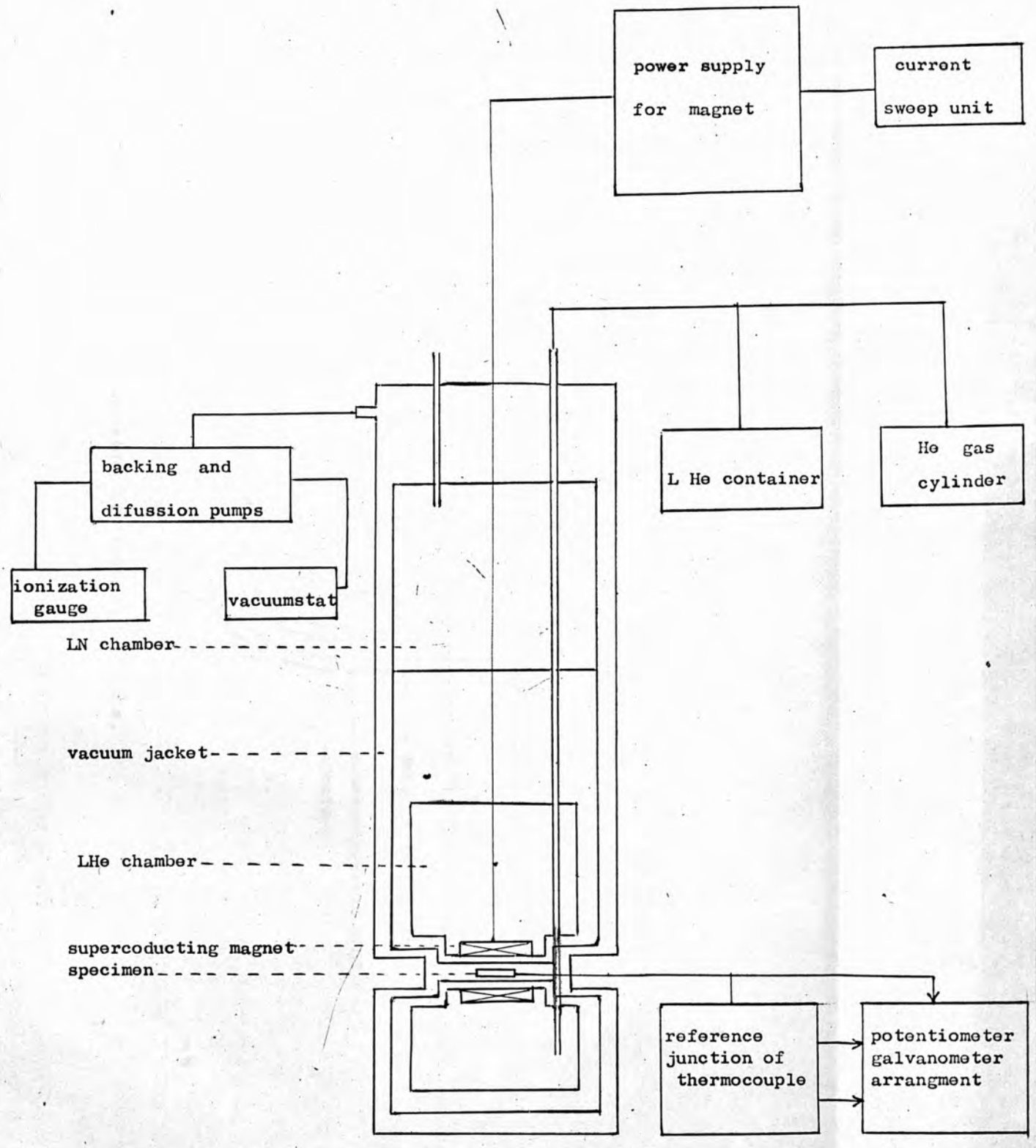

Fig 25 Apparatus for the study of Gurevich-Firsov oscillations (cryomagnetic system G-452).

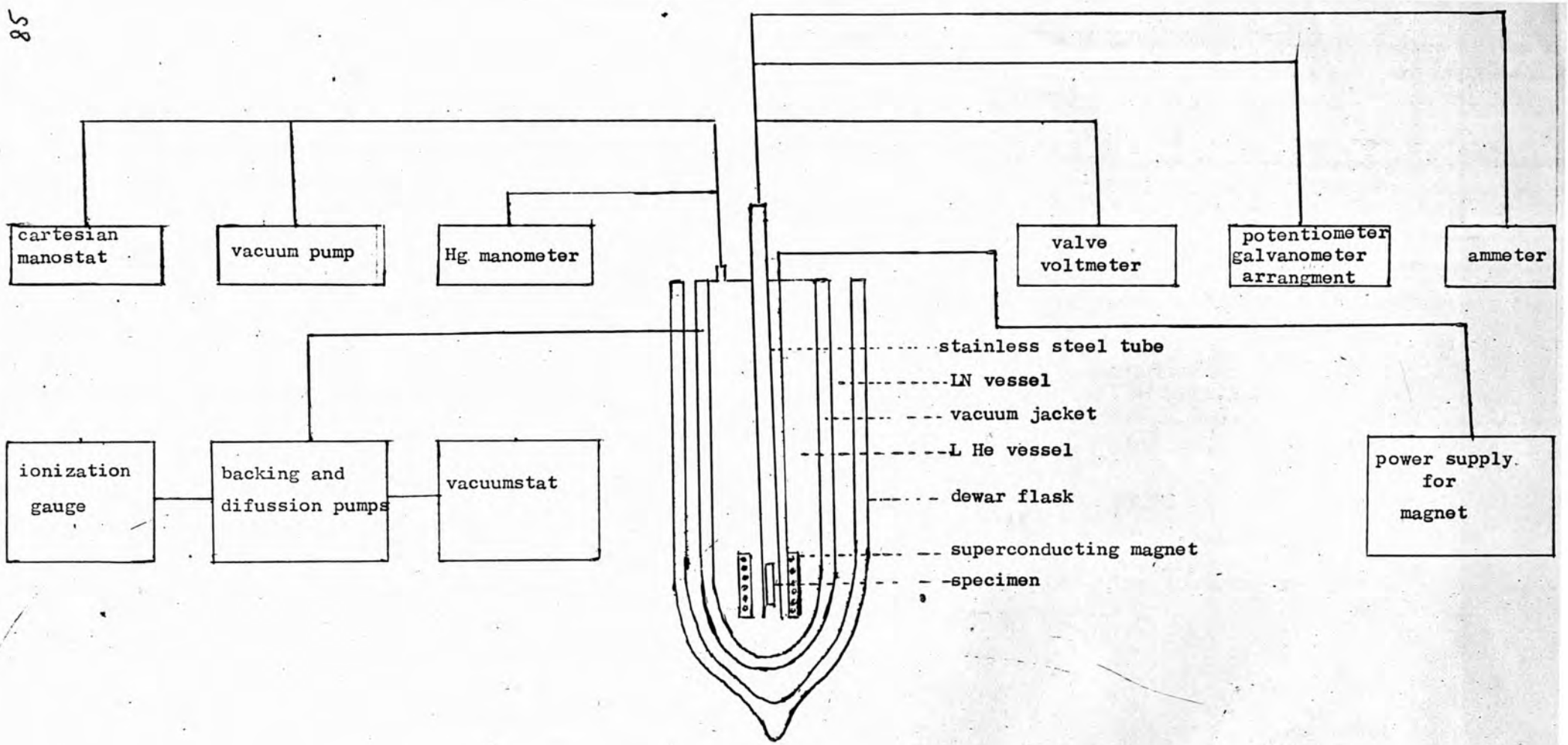

Fig.26 Apparatus for the study of freeze out effects.

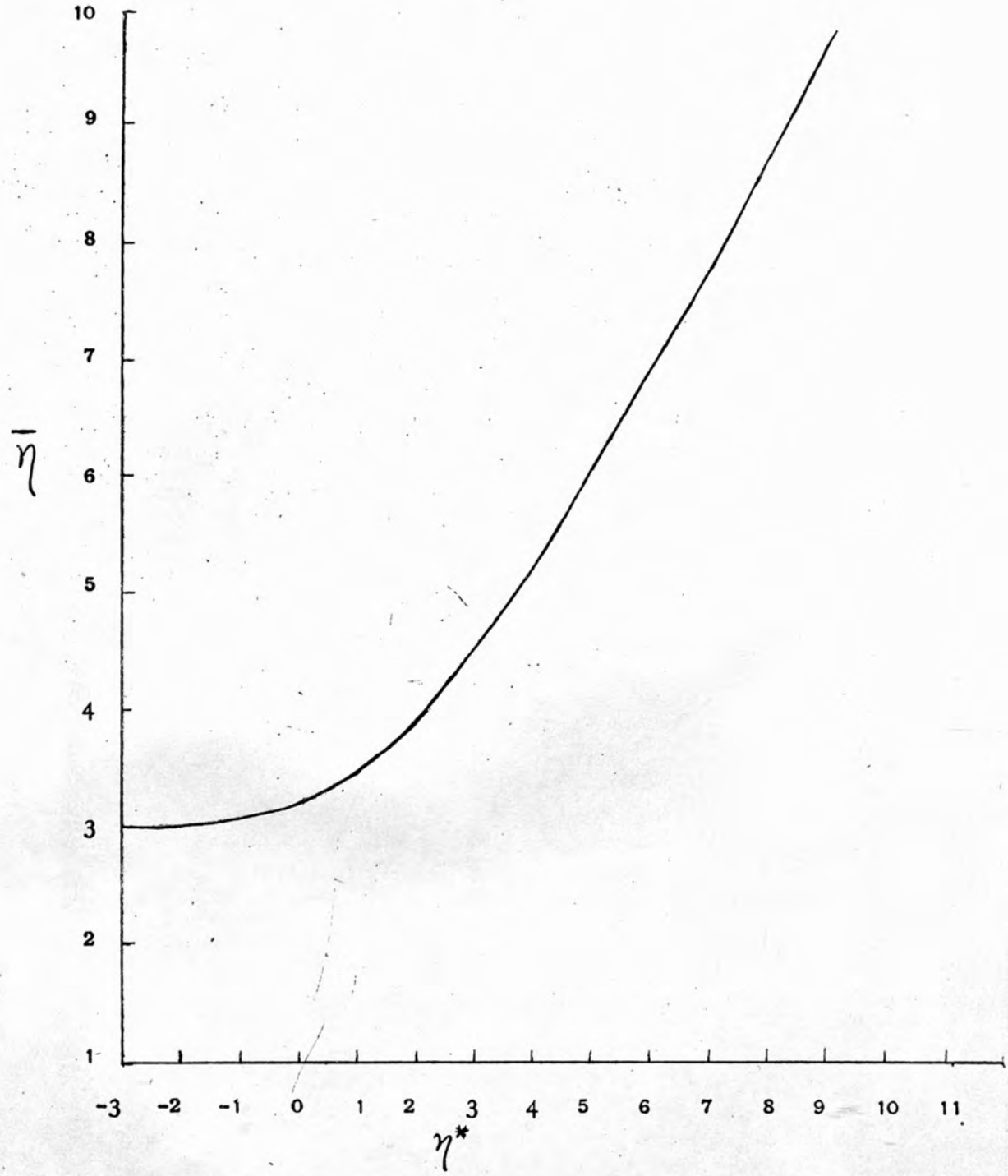

Fig.27 η^* vs. $\bar{\eta}$ (After R. Mansfield 56-M1)